

RESEARCH ARTICLE

Profiling DNA break sites and transcriptional changes in response to contextual fear learning

Ryan T. Stott^{1,2}, Oleg Kritsky^{1,2}, Li-Huei Tsai^{1,2*}

1 Picower Institute for Learning and Memory, Massachusetts Institute of Technology, Cambridge, MA, United States of America, **2** Department of Brain and Cognitive Sciences, Massachusetts Institute of Technology, Cambridge, MA, United States of America

* lhtsai@mit.edu



OPEN ACCESS

Citation: Stott RT, Kritsky O, Tsai L-H (2021) Profiling DNA break sites and transcriptional changes in response to contextual fear learning. PLoS ONE 16(7): e0249691. <https://doi.org/10.1371/journal.pone.0249691>

Editor: Bing Yao, Emory University, UNITED STATES

Received: March 16, 2021

Accepted: May 27, 2021

Published: July 1, 2021

Peer Review History: PLOS recognizes the benefits of transparency in the peer review process; therefore, we enable the publication of all of the content of peer review and author responses alongside final, published articles. The editorial history of this article is available here: <https://doi.org/10.1371/journal.pone.0249691>

Copyright: © 2021 Stott et al. This is an open access article distributed under the terms of the [Creative Commons Attribution License](https://creativecommons.org/licenses/by/4.0/), which permits unrestricted use, distribution, and reproduction in any medium, provided the original author and source are credited.

Data Availability Statement: All sequencing data used in this manuscript can be found in the Gene Expression Omnibus repository; sequencing generated for this manuscript can be found at accession number GSE155095 and previously

Abstract

Neuronal activity generates DNA double-strand breaks (DSBs) at specific loci *in vitro* and this facilitates the rapid transcriptional induction of early response genes (ERGs). Physiological neuronal activity, including exposure of mice to learning behaviors, also cause the formation of DSBs, yet the distribution of these breaks and their relation to brain function remains unclear. Here, following contextual fear conditioning (CFC) in mice, we profiled the locations of DSBs genome-wide in the medial prefrontal cortex and hippocampus using γ H2AX ChIP-Seq. Remarkably, we found that DSB formation is widespread in the brain compared to cultured primary neurons and they are predominately involved in synaptic processes. We observed increased DNA breaks at genes induced by CFC in neuronal and non-neuronal nuclei. Activity-regulated and proteostasis-related transcription factors appear to govern some of these gene expression changes across cell types. Finally, we find that glia but not neurons have a robust transcriptional response to glucocorticoids, and many of these genes are sites of DSBs. Our results indicate that learning behaviors cause widespread DSB formation in the brain that are associated with experience-driven transcriptional changes across both neuronal and glial cells.

Introduction

Neuronal activity has been reported to generate DSBs [1–6]. This was initially observed in cultured neurons, where a well-known marker of DSBs, γ H2AX (phosphorylation on serine 139 of histone H2A variant X [7]), rapidly increased following glutamate receptor activation [2]. Subsequently, stimulation of the rodent brain was found to generate DSBs following seizures [5] or behavioral manipulation [1, 3]. While wakefulness in zebrafish [4], or wakefulness with exploration in fruit flies and mice [8], increased DSBs in neurons that were reduced during sleep.

One source of genomic stress in the brain is its high transcriptional output; neurons respond in real-time to environmental changes and this activity necessitates continual modulation of transcription [9]. We made the unexpected discovery that stimulating the activity of

published sequencing can be found at accession number GSE74971.

Funding: This work was supported by research grants from National Institutes of Health <https://www.nih.gov/> (R01NS102730-01), the Glenn Foundation for Medical Research <https://glennfoundation.org/> and the JPB Foundation <https://www.jpbfoundation.org/> to LHT. RS was the recipient of the MIT Presidential Fellowship, the Barbara Weedon Fellowship, and the Lord Foundation Fellowship. The funders had no role in study design, data collection and analysis, decision to publish, or preparation of the manuscript.

Competing interests: The authors have declared that no competing interests exist.

primary cortical neurons generates DSBs specifically at the rapidly induced early response genes (ERGs), and this promotes their expression [3]. Increases in γ H2AX at some of these ERGs was later observed in the brain during fear learning [6] or following memory retrieval [10]. In other contexts of gene induction, including through transcriptional induction mediated by nuclear receptors [11–14] or heat shock and serum-stimulation [15], DSBs appear to facilitate gene induction. Within the complex milieu of the brain, it is therefore likely that different upstream pathways contribute to the generation of DSBs, yet their locations and their relation to brain function is an open question. As DSBs pose a threat to genomic integrity [3], understanding the genome-wide DSB landscape of the brain would facilitate our understanding of how the brain balances timely transcriptional responses with the generation of DSBs, while revealing sites of genomic stress that could seed DNA lesions detrimental to neuronal function and contribute to brain aging and neurodegenerative diseases.

We set out to understand the *in vivo* landscape of DSBs in the brain during learning and how they correspond with gene expression changes occurring in neurons and glia. We find fear learning paradigm-induced genes are overrepresented amongst those genes with the highest levels of DSBs in the medial prefrontal cortex and hippocampus. These genes are downstream of pathways that are shared in part by neurons and non-neurons, and in other cases unique to each group of cells. Surprisingly, we find potential glia-enriched DSB hotspots at genes that have a robust transcriptional response to glucocorticoid receptor signaling in glia.

Results

Fear learning induces DNA double-strand breaks in the brain

Increases in neuronal activity result in the formation of DSBs both *in vitro* and *in vivo* [1, 3]. However, it was unclear whether DSBs form at specific genomic loci in the brain and in which cell types in response to a normal physiological event. To elicit neuronal activation in a physiologically relevant manner, we utilized contextual fear conditioning (CFC), which generates a strong associative memory between a novel environment and an aversive stimulus, a foot shock [16]. We assessed neuronal activation in the hippocampus (HIP) and the medial prefrontal cortex (mPFC) of adult wild-type male C57BL/6J mice, two brain regions known to be recruited during CFC for subsequent memory formation [16]. Induced expression of ERGs (e.g., *Npas4*, *Arc*) is known to rapidly follow neuronal activation [3]. Indeed, we found induction of these genes in both brain regions 30 minutes after CFC, with higher induction in the mPFC (S1A Fig).

Chromatin immunoprecipitation sequencing (ChIP-Seq) for γ H2AX, a chromatin marker of DSBs [7], is a sensitive method for identifying DSBs genome-wide [3, 17–20]. We performed γ H2AX ChIP-Seq 30 minutes following CFC to measure the formation of DSBs. In the naive hippocampus we observed 136 γ H2AX peaks, increasing to 280 γ H2AX peaks after CFC, with 125 peaks shared between conditions (S2 Table). In the naive mPFC we observed 120 γ H2AX peaks, increasing to 255 γ H2AX peaks after CFC, with 102 peaks shared between conditions (S2 Table). Including all peaks called under the naive and CFC conditions, we found 291 γ H2AX peaks annotated to 323 genes in hippocampus, and 273 γ H2AX peaks annotated to 306 genes in mPFC (Fig 1A; S1B Fig; S2 Table). Consistent with previous studies, γ H2AX peaks were located at gene bodies and proportional to gene length, yet often stretching past the 3'-UTR (S1C Fig) [3, 15, 17].

There was a large overlap between γ H2AX peaks called in both hippocampus and mPFC, reflecting their shared recruitment during learning (Fig 1A). We utilized clusterProfiler [21] to perform gene ontology (GO) analysis of these 206 γ H2AX peak-containing genes and clustering of the top biological processes yielded four unique categories (S1D Fig). The largest cluster

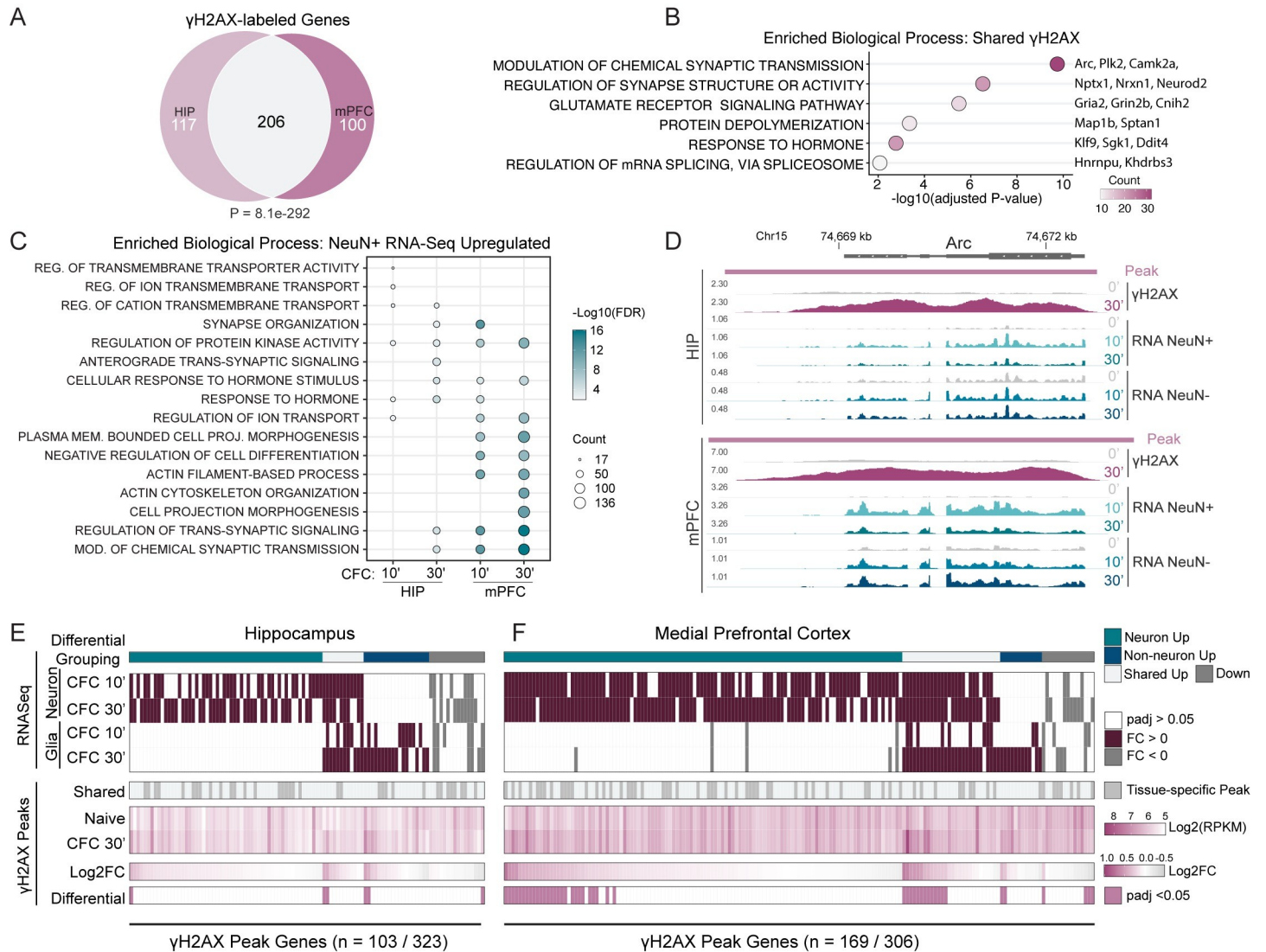


Fig 1. Fear learning induces DNA double-strand breaks in the brain. (A) Venn diagram of the γ H2AX peak-containing genes shared between HIP and mPFC for both naive and CFC conditions. P-value calculated using hypergeometric distribution test. (B) Six representative top biological processes for the 206 γ H2AX peak-containing genes shared between HIP and mPFC in (A). Over-representation analysis with gene ontology (GO) category “Biological Process.” (C) The top 5 biological processes for the CFC-upregulated genes in NeuN+ nuclei at each 10- and 30-minute timepoint. Over-representation analysis with gene ontology (GO) category “Biological Process.” (D) Genome browser tracks for the gene *Arc*. Both HIP and mPFC are shown. Whole tissue γ H2AX ChIP-Seq is shown as LogLR signal tracks (“ γ H2AX”). Signal normalized total RNA-Seq from FACS-isolated nuclei is shown for neurons (“RNA NeuN+”) and non-neurons (“RNA NeuN-”). Time points following contextual fear conditioning are noted; naive, 10, and 30 minutes (0’, 10’, 30’). γ H2AX ChIP-seq tracks are the combined signal for 3–4 independent replicates, each replicate generated from the pooling of 3 animals. RNA-Seq tracks are the combined signal for 3–4 independent replicates. (E-F) Heatmaps of the genes containing γ H2AX peaks that sustained transcriptional regulation after CFC. RNA-Seq heatmap denotes differential genes (“RNA-Seq”) and color bar (“Differential Grouping”) denotes cell type specificity. The γ H2AX heatmaps show peaks shared between tissues (“Shared”), RPKM of γ H2AX signal, Log2FC, and those peaks changing after CFC with $padj < 0.05$ (“Differential”). Left is hippocampus (E), Right is mPFC (F).

<https://doi.org/10.1371/journal.pone.0249691.g001>

contained those GOs related to synaptic function (e.g., ‘modulation of chemical synaptic transmission’) that included glutamate receptors *Gria2* and *Grin2b*, synaptic plasticity regulators like *Camk2a* [22], and ERGs like *Arc* [23] and *Plk2* [24] (Fig 1B). Similar to a previous report in the immune setting, many of these genes are lineage-specific, like the transcription factor *Neurod2* [17]. Two clusters composed of single GO terms were observed, one enriched for RNA binding genes (‘Regulation of mRNA splicing, via spliceosome’) and one enriched for

cytoskeleton-related genes ('protein depolymerization') (Fig 1B). Finally, the fourth unique cluster was related to hormone or biological rhythms (e.g., 'response to hormone') (Fig 1B). To confirm γ H2AX peaks at ERGs, we performed γ H2AX ChIP-qPCR on pooled hippocampi collected 30 minutes following CFC. Compared to the naive condition, hippocampi of CFC mice had significant increases in γ H2AX at the gene bodies of the ERGs *Npas4* and *Nr4a1*, but not at the housekeeping gene *B2m* (S1E Fig). These findings indicate that many genes essential for neuronal function and memory formation, and significantly more of them than expected based on previous observations in cultured neurons following NMDA stimulation, are potentially hotspots of DSB formation. As DSBs represent a grave threat to genomic integrity [25], with its sequela including transcriptional dysregulation and genomic rearrangements, this suggests that genes critical for neuronal function are uniquely vulnerable to DNA damage.

We previously observed that the formation of DSBs correlated with rapid gene induction in neurons, particularly the ERGs which we find are sites of DSBs in the brain. To understand how these DSBs correlate with CFC-induced gene expression changes, we performed nuclear RNA-Seq. While whole-cell mRNA levels reflect both RNA synthesis and RNA degradation, assaying nuclear RNA levels more directly measures transcriptional activity. We fixed and enriched for neuronal and non-neuronal nuclei collected 10 and 30 minutes after CFC through fluorescence-activated cell sorting (FACS), using the pan-neuronal nuclei marker NeuN [26] (S2A Fig). Nuclei were decrosslinked after sorting and total RNA was isolated for downstream analysis. Utilizing an intronic primer, we found higher transcriptional induction of the neuron-specific ERG *Npas4* [27] in the FACS-isolated neuronal (NeuN+) nuclear RNA than whole mPFC lysate, with minimal expression in the non-neuronal (NeuN-) fraction, indicating successful purification of neurons and non-neurons (S2B Fig). Assaying mRNA of the canonical ERG *Arc* showed induction in both neuronal and non-neuronal nuclei following CFC (S2B Fig). Because the peak of ERG induction occurred as early as 10 minutes or as late as 30 minutes after CFC, we included both time points in our sequencing analyses (S2B Fig).

We next performed nuclear RNA-seq of sorted neurons and non-neurons 10 and 30 minutes subsequent to CFC. First, successful isolation of neuronal nuclei was validated by examining aggregate expression of known cell type-enriched genes [28], finding that pyramidal- and interneuron-enriched genes were highly correlated with the NeuN+ RNA-Seq, while genes enriched in glia, including astrocytes, microglia, and oligodendrocytes, along with other non-neuronal cells were strongly enriched in the NeuN- RNA-Seq (S3A Fig). We identified hundreds of upregulated genes, indicating that fear learning activates the transcriptomes of neurons and non-neurons across brain regions within minutes (S3B–S3E Fig; S3 Table). The mPFC had the highest number of upregulated genes, suggesting a stronger transcriptional response in this area during learning (S3F Fig). In agreement with our γ H2AX ChIP-seq analysis, there was a large overlap between HIP and mPFC upregulated genes in neurons (202 genes at 10 minutes and 448 genes at 30 minutes) (S3F Fig). Non-neuronal nuclei also exhibited considerable transcriptional changes in response to CFC, but with more comparable numbers of upregulated genes between brain areas and with a large overlap occurring at 30 minutes (34 genes at 10 minutes and 242 genes at 30 minutes) (S3G Fig). Further, we found biological processes related to synaptic structure and function were amongst the most enriched GO categories in the upregulated genes of neurons—mirroring our γ H2AX ChIP-Seq (Fig 1C). In contrast, neuronal downregulated genes had minimal enrichment for biological processes (a single significantly enriched term: "cell-cell adhesion via plasma-membrane adhesion molecules"; adjusted p-value = 2.4×10^{-3}).

To assess the relationships between activity-induced DSBs and gene expression in the brain, we compared the ChIP-seq and RNA-seq data. First, examining a specific genomic locus of the ERG *Arc* revealed increases in γ H2AX signal with concomitant upregulation in

both neurons and non-neurons (Fig 1D). Globally, we find four categories of γ H2AX-associated genes whose expression was altered after CFC: those upregulated exclusively in neurons (56 HIP and 114 mPFC), genes upregulated in both neurons and non-neurons (12 HIP and 28 mPFC), genes upregulated specifically in non-neurons (19 HIP and 12 mPFC), and a small subset of downregulated genes (16 HIP and 15 mPFC) (categories denoted by “Differential Grouping” row) (Fig 1E and 1F). Overall, we find transcriptional changes are more strongly associated with γ H2AX in the brain than anticipated. Previously, we observed twenty gene-associated γ H2AX loci following stimulation of cultured neurons [3], while in the HIP and mPFC we see more than 100–150 gene-associated γ H2AX loci that are transcriptionally induced (Fig 1E and 1F).

Activity-dependent genes are a source of DNA breaks in the brain

We next sought to understand the overlap between CFC-upregulated genes and γ H2AX peaks. Overall, we found that γ H2AX peaks were over-represented with genes upregulated by fear learning, particularly in the mPFC where we saw higher induction of gene expression (Fig 2A and S4A Fig). However, absolute transcription level is known to correlate with DSBs in both human and mouse cells [29–31]. By binning all expressed genes at the CFC30' time point in

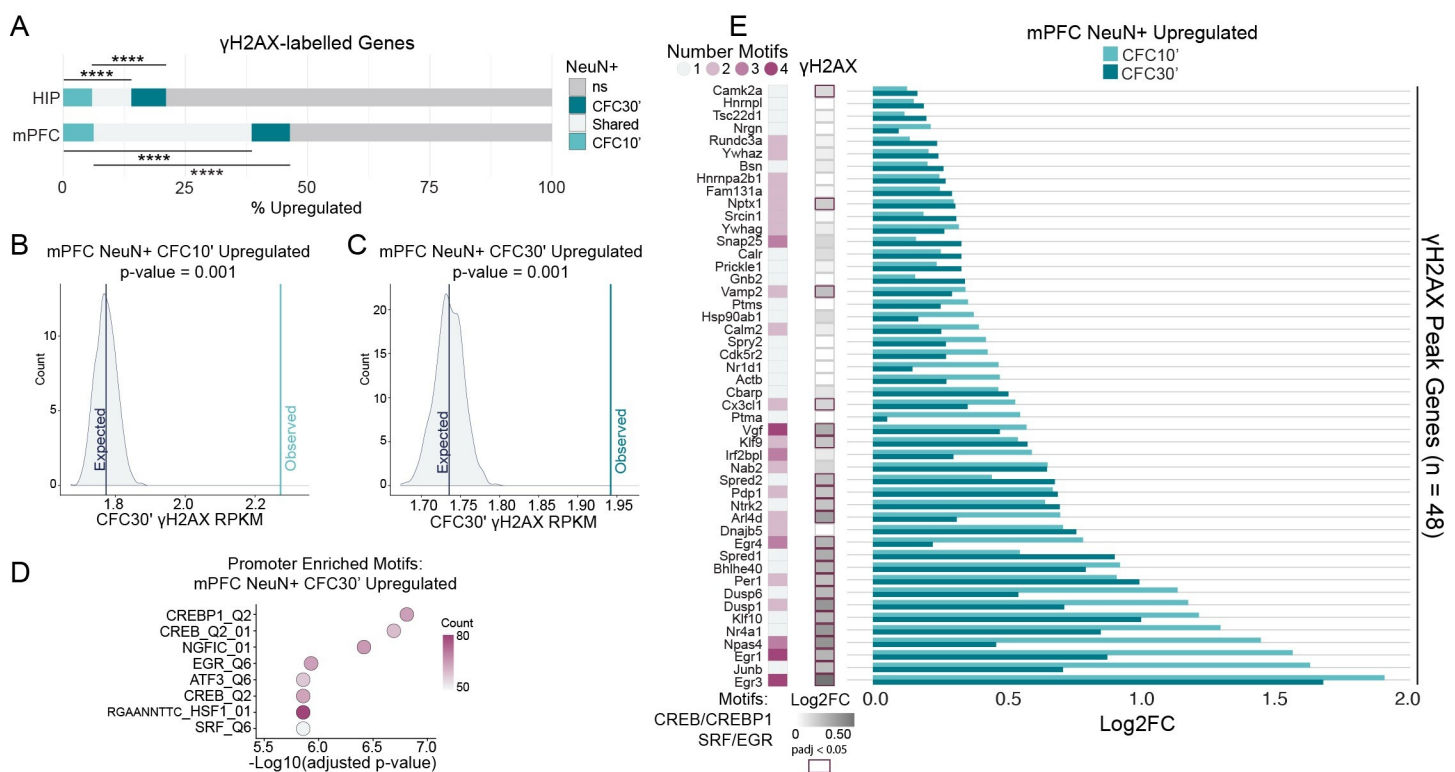


Fig 2. Activity-dependent genes are a source of DNA breaks in the brain. (A) Percent overlap between genes containing a γ H2AX peak and those that were upregulated ($\text{padj} < 0.05$) in neuronal nuclei after CFC. Hypergeometric distribution test; **** $P < 0.0001$. (B–C) Permutation testing to assess whether CFC-upregulated genes at 10 minutes (B) or 30 minutes (C) have greater than expected γ H2AX intensity, accounting for RNA expression level at the same time point (CFC30'). Distributions show the mean γ H2AX intensity (RPKM) for 1000 permutations of random sampling, binned by RNA expression level (FPKM). Lines are the mean γ H2AX RPKM of either all permutations (“Expected”), or genes upregulated at the specified time point (“Observed”). (D) Top 8 enriched promoter motifs for the genes upregulated in neuronal nuclei from mPFC 30 minutes after CFC ($\text{Log}_2\text{FC} > 0$ & $\text{FDR} < 0.05$). Using the “Transcription Factor Targets” (TFT) gene set from the molecular signatures database (MSigDB). (E) Select activity-associated motifs at the promoters of 48 upregulated genes with DSBs. Left, number of the specified motifs associated with each gene’s promoter. Center, γ H2AX Log_2FC , right, fold change observed after CFC in mPFC NeuN+ nuclei. Using the TFT gene sets from MSigDB for each transcription factor motif.

<https://doi.org/10.1371/journal.pone.0249691.g002>

the mPFC by expression level, we observed that genes with higher RNA expression had higher γ H2AX levels in the gene body (S4B Fig). This potentially explains some of the ~55% of the γ H2AX-associated genes in the mPFC and ~80% in the HIP that are non-responsive to CFC (Fig 2A).

We next asked whether upregulated genes have higher amounts of γ H2AX than can be explained simply by their transcription level alone. Using permutation testing, we binned neuronal upregulated genes by RNA expression level, and these bins were then used for random sampling without replacement from all expressed genes. We found upregulated genes have higher γ H2AX intensity than would be expected by their transcriptional level (Fig 2B and 2C and S4C Fig). Further, the more rapid the induction (CFC 10 minutes) the greater the discrepancy between the observed and the expected γ H2AX level (Fig 2B and 2C). Thus, while many of the observed sites of DSBs may reflect high expression levels, as exemplified by non-induced highly expressed housekeeping genes like histone genes or neuronal lineage genes (S2 Table), gene induction also appears to correlate with increased γ H2AX.

To understand what pathways were mediating the rapid induction of gene expression following CFC in neurons, we searched for transcription factor motif overrepresentation at the promoters of differentially expressed genes, using the Molecular Signatures Database (MSigDB) [32]. Motifs from CREB/ATF family members, EGR family members, as well as SRF, were all enriched (Fig 2D and S5A–S5C Fig). These transcription factors are known to act downstream of cellular activation and calcium influx, including through MAPK signaling [23]. Examining all upregulated genes associated with CREB/ATF, EGR, and SRF motifs for the presence of γ H2AX enrichment yields 48 genes in mPFC and 20 genes in HIP (Fig 2F and S5D Fig). Importantly, a number of these activity regulated genes, such as *Npas4*, *Fos*, *Nr4a1*, *Actb*, *Ntrk2*, and *Egr1* are known to be targets of these transcription factors, and are essential for efficient memory formation after CFC [13, 33–37]. Other genes that fit the same category, including *Arc* and *1700016P03Rik* (mir212/mir132) were not included because their regulatory motifs are not in the close vicinity of the TSS [38–40].

Having established a connection between rapid gene induction and γ H2AX foci in the brain, we next wanted to understand if any of our DSBs are likely to correspond to late response genes, the second wave of genes induced following stimulation [41]. We compared the observations in the mPFC to a published single-cell RNA-Seq dataset which measured cell-type-specific induction of early-response genes ($n = 350$) and late-response genes ($n = 251$) after light stimulation of the visual cortex [42]. We found that the rapidly induced early-response genes are enriched with our mPFC DSB-labeled genes (S6 Fig), with *Tuba1a* the only γ H2AX site that is exclusively upregulated at the late-response time point (S6 Fig). This suggests that we are not missing DSBs that occurred at late response genes and recapitulates our nuclear RNA-Seq findings with single cell mRNA. Altogether, these results indicate that DSB formation is more widespread in the brain than previously documented and is associated with an important subset of transcriptionally upregulated genes following CFC.

Fear learning induces a proteostasis response in neurons and non-neurons

We observed a number of γ H2AX-associated genes whose expression was altered after CFC in both neurons and non-neurons (Fig 1E). These included early genes (e.g., *Arc*, *Egr1*) and chaperones (e.g., *Hsp90ab1*, *Hspa8*). We had also observed the heat shock transcription factor HSF1, which induces genes in response to protein folding stress [43], enriched in the promoters of neuronal upregulated genes in both HIP and mPFC (Fig 2D and S5A and S5C Fig). Transcription factor motif analysis of the promoters of genes upregulated in non-neuronal nuclei 30 minutes after CFC yielded both HSF1 and the activity-regulated transcription factor

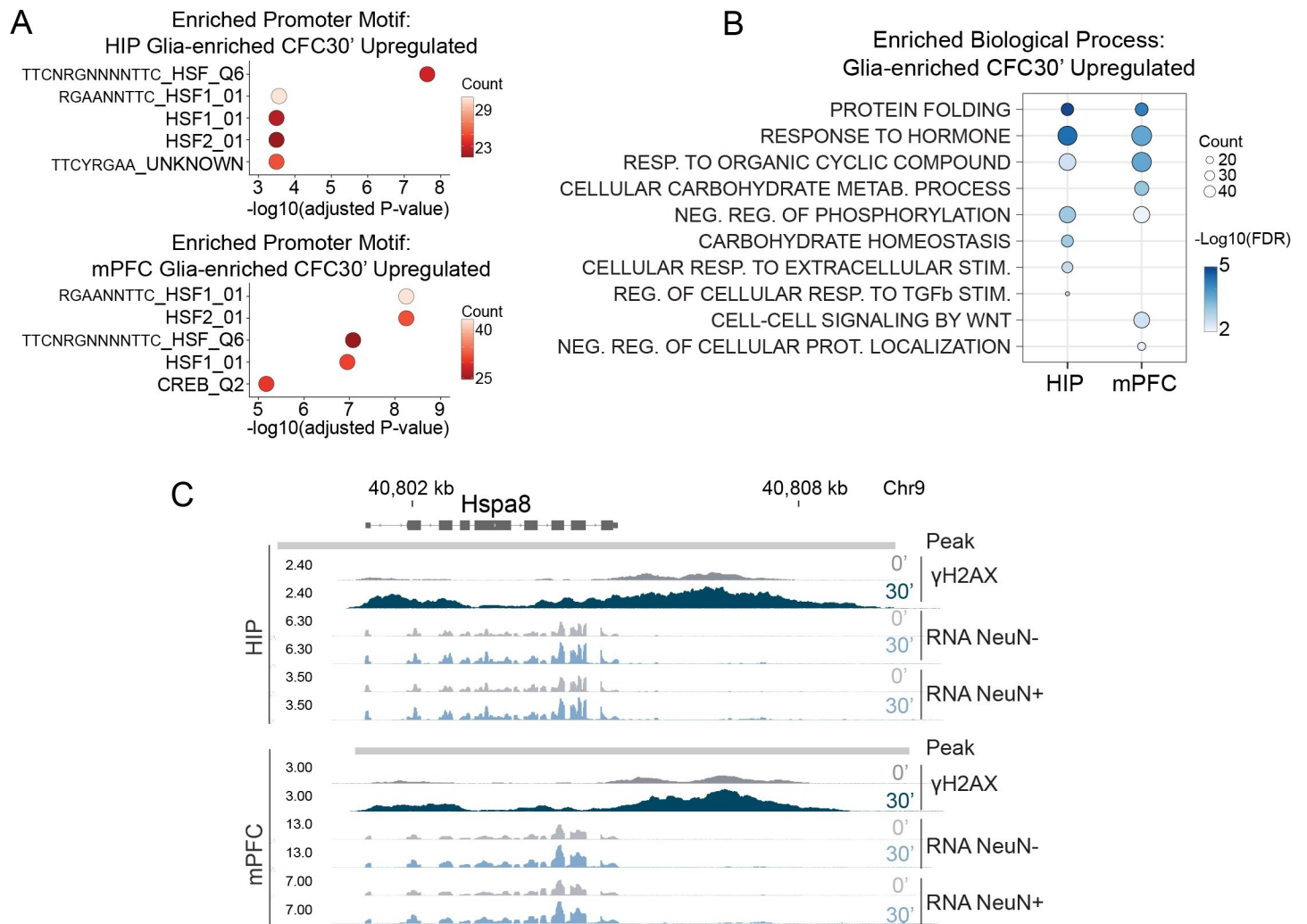


Fig 3. Fear learning induces a proteostasis response in neurons and non-neurons. (A) Top 5 enriched promoter motifs at the genes upregulated in HIP NeuN- nuclei (top) and mPFC NeuN- nuclei (bottom) 30 minutes after CFC. Using the TFT gene sets from MSigDB for each transcription factor motif. (B) Ten representative top enriched biological processes for non-neuronal nuclei 30 minutes after CFC. Enrichment for the 426 upregulated genes in HIP and 511 upregulated genes in mPFC. Over-representation analysis with GO category "Biological Process." (C) Genome browser tracks for the chaperone *Hspa8*.

<https://doi.org/10.1371/journal.pone.0249691.g003>

CREB, as in neurons (Fig 3A). Indeed, a number of the CFC-induced genes in non-neuronal nuclei appear to be activity-regulated (S7A Fig). Activation of astrocytes during learning is known to be important for memory formation [44], and these rapid transcriptional responses mediated by activity-regulated transcription factors may reflect an important role of glia in the response to fear learning. We next examined clustering of the top GO terms from these non-neuronal genes and found biological processes related to protein folding, hormone response, metabolism, and signaling (Fig 3B and S7B and S7C Fig). This indicates that CFC elicits a protein folding response and cellular activity-regulated response which is shared by multiple cell types. Inspecting signal tracks for the HSP70 family member *Hspa8* highlighted this relationship, showing the presence of an inducible γ H2AX peak (S1B Fig) and increased RNA expression after CFC in both neurons and non-neurons (Fig 3C). Confirming increased HSF1 activity following CFC, we found increased nuclear HSF1 in neurons and non-neurons following CFC, and increased binding of HSF1 to the promoters of *Hsp90ab1* and *Hspa8* (S8A and S8B Fig).

In HIP and mPFC we found multiple genes with γ H2AX peaks that were induced after CFC and which are potential HSF1 targets because of promoter HSF1 binding following heat shock in mouse embryonic fibroblasts [45] (HIP: *Hspa8*, *Baiap2*, *Sh3gl1*, *Dnaja1*, *Hsp90ab1*, *Dynll1*, *Mbp*, *Ywhah*, *Dnajb5*, *Ddit4*, *Prkag2*, *Gse1*, *Ptk2b*, *Arpc2*, *Ywhag*; mPFC: *Tcf4*, *Hspa8*, *Baiap2*, *Hsp90ab1*, *Hnrnpa2b1*, *Gfod1*, *Lncpint*, *Ywhah*, *Dnajb5*, *Ddit4*, *Ywhag*). We also identified ATF6, which functions as part of the unfolded protein response (UPR) and facilitates protein quality control in the endoplasmic reticulum [46], as a potential regulator of additional genes. Known ATF6 targets such as *Hspa5* (Grp78) [47], *Calr* [47], *Xbp1* [48], and others (*Ywhaz*, *Atp2b1*) [49], were enriched with γ H2AX peaks and upregulated in neurons and to a lesser degree non-neurons. These findings indicate that CFC generates a rapid proteostasis response in both neurons and non-neurons, with induced genes constituting sites of DNA breaks.

Glucocorticoid-regulated genes are sites of DNA double-strand breaks

'Response to hormone' was one of the top enriched biological processes observed amongst the CFC-induced genes in non-neuronal nuclei (Fig 3B) as well as the γ H2AX peaks (Fig 1B). Examining these genes further, we found examples such as *Sgk1* and *Ddit4* which are known to be regulated by the glucocorticoid receptor (GR) [50, 51] and while not upregulated in neuronal nuclei, were upregulated at the mRNA level in whole HIP and mPFC lysate (Fig 4A and S9A Fig). Unlike neuronal activity, which occurs immediately upon exposure to environmental changes, the hormonal response to stress is delayed while the signal is relayed through the hypothalamic-pituitary-adrenal axis, before eliciting glucocorticoid release into the blood stream. Glucocorticoids increase in the blood within 30 minutes following exposure to a stressor [52], corresponding with increases in the intrahippocampal corticosterone concentration [53] and nuclear localization of the GR in the mouse brain [52]. We observed that 30 minutes was the time point where non-neuronal CFC-upregulated genes were most likely associated with a γ H2AX peak (Fig 4A). Furthermore, compared to other brain areas, the mPFC and HIP have some of the highest expression of GR [54], suggesting they are key targets of the stress response. To identify putative GR-regulated genes, we utilized two ChIP-Seq datasets of GR binding in rat cortex to map all binding sites containing the glucocorticoid-responsive element (GRE) in the mouse genome to the nearest gene (S4 Table) [55, 56]. Interestingly, we found that many of the γ H2AX-containing genes that were responsive to CFC only in non-neuronal nuclei are coincident with genes annotated to a GR-binding site (Fig 4A).

We tested whether a subset of these genes can be induced by the GR-specific agonist dexamethasone in cultured primary glia. In contrast to *Actb* which is not a known target of GR, we found dexamethasone induced the expression of *Ddit4*, *Sgk1*, and *Glul*, genes that were specifically upregulated in non-neuronal nuclei during CFC and annotated to a GR-binding site (Fig 4B). Thus, our findings implicated the GR in mediating gene induction in glia after fear learning. Next, to assess whether GR activity is sufficient to increase DSBs at these genes, we treated cultured primary glia with dexamethasone and measured γ H2AX enrichment by ChIP-qPCR. The genes *Ddit4*, *Glul*, and *Sgk1*, alongside the canonical GR-inducible gene *Mt1* [58], showed significant increases in γ H2AX enrichment (Fig 4C). *Arc*, with similarly high γ H2AX levels following CFC, alongside the housekeeping gene *B2m*, did not exhibit γ H2AX enrichment in response to dexamethasone (S9B Fig).

Our RNA-seq data from sorted nuclei showed upregulation of the γ H2AX-associated gene *Ddit4* only in non-neuronal nuclei following CFC, a similar pattern for many of our other putative and confirmed GR-regulated genes (Fig 4D). To understand whether non-neurons had more active GR-bound enhancers, we utilized a ChIP-Seq dataset of histone 3 lysine 27

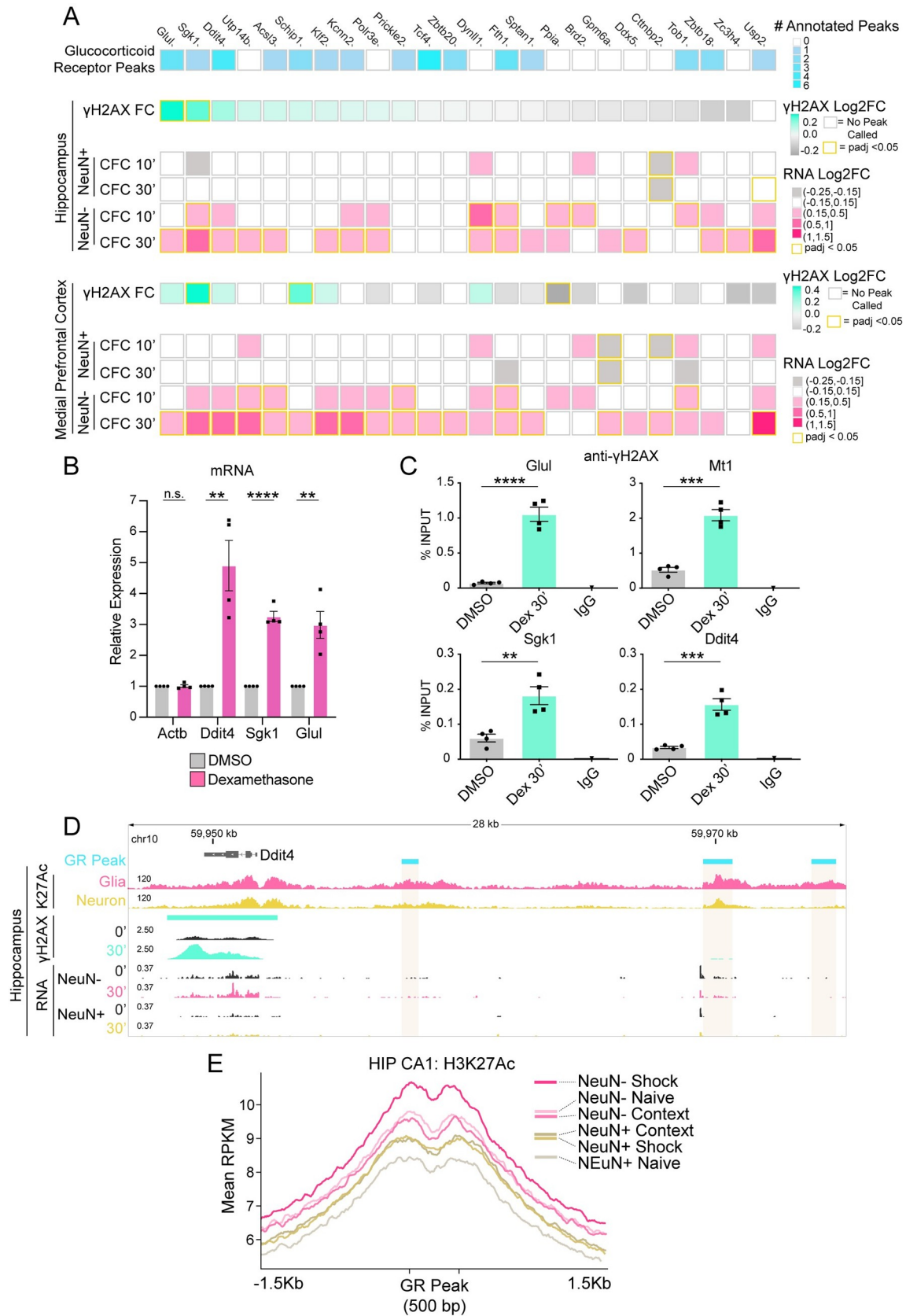


Fig 4. Glucocorticoid-regulated genes are sites of DNA double-strand breaks. (A) Heatmap of γ H2AX peaks occurring at genes upregulated specifically in non-neuronal nuclei. Top, number of glucocorticoid receptor binding sites annotated per gene (rat cortical ChIP-Seq) [55, 56]. γ H2AX Log2FC and upregulated genes for HIP and mPFC after CFC. (B) RT-qPCR analysis of mRNA induction in mouse glial primary cultures 2 hours after treatment with glucocorticoid receptor agonist dexamethasone (100nM). N = 4 independent cultures; two-tailed unpaired student's t-test; **P \leq 0.01; *** P \leq 0.001; **** P $<$ 0.0001; Mean \pm SEM. (C) ChIP-qPCR analysis of γ H2AX induction at select gene bodies in mouse glial primary cultures 30 minutes after treatment with dexamethasone (Dex) (100nM). N = 4 independent cultures; two-tailed unpaired student's t-test; **P \leq 0.01; *** P \leq 0.001; **** P $<$ 0.0001; Mean \pm SEM. (D) Genome browser snapshot of the gene *Ddit4*. Top, glucocorticoid receptor binding sites ('GR Peak'; rat cortical ChIP-Seq) [55, 56], hippocampal region CA1 H3K27ac ChIP-Seq from NeuN+ or NeuN- isolated nuclei 1 Hour after CFC ('K27Ac') [57], γ H2AX LogLR signal tracks, and nuclear RNA-Seq. (E) Average H3K27ac signal at glucocorticoid receptor binding sites (rat cortical ChIP-Seq) [55, 56] containing the GR motif in mouse (n = 5591 peaks). H3K27ac ChIP-Seq of mouse hippocampal CA1 region from NeuN+ or NeuN- isolated nuclei 1 hour after exposure to context, or CFC ('shock') [57]. Colored bars represent the apex of each condition.

<https://doi.org/10.1371/journal.pone.0249691.g004>

acetylation (H3K27Ac), a chromatin mark of enhancer and promoter activity, from purified neuronal and non-neuronal nuclei [57]. Glia have higher H3K27Ac signal at the GR-bound enhancers surrounding *Ddit4*, indicating that GR-regulated enhancers are more active in non-neuronal nuclei than neurons (Fig 4D). To examine this phenomenon genome-wide, we looked at aggregate H3K27Ac signal in neurons and non-neurons at all GR-binding sites (S4 Table) [55, 56]. Strikingly, both the anterior cingulate cortex (ACC) of the medial prefrontal cortex, and the hippocampal area Cornu Ammonis 1 (CA1) showed higher baseline acetylation around GR peaks in non-neurons vs. neurons ('Naive') (Fig 4E and S9C Fig). We then examined H3K27Ac signal in CA1 under additional experimental conditions including 'context' (exposure to the context without a foot shock) and 'shock' (context paired with a foot shock). We found that H3K27Ac signal at GR peaks in the neuronal fraction increased similarly after exposure to either context or shock, suggesting a generalized enhancer activation in response to exploratory behavior that may be independent of stress. In contrast, the non-neuronal fraction showed increases in H3K27Ac after shock, demonstrating that these enhancers are responsive to the stressful condition in non-neurons but not in neurons (Fig 4E; S9D Fig, intergenic peaks).

Our findings identified a group of CFC-responsive non-neuronal genes that are likely regulated by GR signaling (Fig 4A–4E). We checked gene expression of the GR gene, *Nr3c1*, finding that neurons express *Nr3c1* at approximately half the level of non-neurons (S9E Fig). The differing GR expression levels could be one of the reasons why these same genes did not exhibit induction or increased enhancer activity in neurons (Fig 4A). Therefore, we verified whether GR nuclear translocation occurs in response to receptor agonism in both cell types. We measured GR nuclear intensity in mouse brain after treatment with corticosterone, the predominant glucocorticoid in rodents [59]. We found increases in nuclear GR in both neurons and non-neurons (though there was a trend, it was not significant in the NeuN- fraction) (S9F Fig). Thus, the absence of a neuronal stress-mediated change in enhancer activity is likely due to decreased chromatin accessibility at the enhancer level [60], highlighting that glia may play a significant role in the homeostatic response to stress. Nevertheless, it is unclear whether neurons are capable of mounting a transcriptional response to stress hormone, and whether induction of hormone-responsive genes in neurons would be accompanied by DSBs.

Glia but not neurons have a robust transcriptional response to corticosterone

To test whether an endogenous GR agonist was sufficient to upregulate some of the glial genes displaying elevated levels of γ H2AX and transcription following CFC, we injected mice with corticosterone at a dose known to approximate a stressful experience [61], and collected the hippocampus 30 minutes later. We FACS-sorted nuclei into four cell populations: neuronal

(NeuN+), astrocytic (GFAP+), microglial (PU.1+), and oligodendrocyte-enriched (NeuN-, GFAP-, PU.1-; 3X-), and subjected them to RNA extraction (S10A Fig). RT-qPCR analysis showed enrichment for respective cell type markers, indicating successful isolation of cell types (S10B Fig). We then assessed gene expression changes in *Sgk1* and *Glul* that have CFC-inducible γ H2AX peaks (S2A Fig), and found that except for neurons, all three glial subtypes could respond to an endogenous GR agonist (S10C Fig). While GR agonists are sufficient to induce the putative glucocorticoid-regulated genes seen after CFC both *in vitro* (dexamethasone; Fig 4B) and *in vivo* (corticosterone; S10C Fig), we sought to determine whether these genes are dependent on the GR for CFC-induced changes in expression. We found that whereas pretreatment with a glucocorticoid receptor antagonist RU-486 (mifepristone) [62] blocked CFC-induced transcription of *Sgk1*, *Ddit4*, and *Glul* in whole hippocampal lysates, it did not alter transcription of the housekeeping gene *Gapdh*, or induction of the ERG *Arc* (Fig 5A).

We next performed RNA-Seq from hippocampal cell types after corticosterone treatment to better understand how the transcriptomes of the four major brain cell types respond to GR-mediated transcriptional regulation. Successful isolation of brain cell types was validated by examining aggregate expression of known cell type-enriched genes [28] (S11A Fig). Neurons have a modest transcriptional response following corticosterone treatment (112 genes; Fig 5B and S11B Fig; S3 Table). In contrast, astrocytes, oligodendrocyte-enriched, and microglia have hundreds of upregulated genes (276, 453, and 551 respectively; Fig 5B and S11C–S11E Fig; S3 Table). Our results are consistent with published *in vitro* findings that reported extensive response to dexamethasone in cultured astrocytes but little in cultured neurons [63]. The ability of glia to mount a robust transcriptional response to glucocorticoids suggests that glia may have a much larger role to play in the response to stress and its impact on the brain during learning than previously appreciated.

Clustering of the top GO terms from the genes upregulated following corticosterone treatment shows major categories of biological processes pertaining to proliferation, cell death, cellular motility, homeostasis, signaling, inflammation, other various cellular functions, and as would be expected, a glucocorticoid response (Fig 5C; S12A–S12C Fig). No enriched terms were observed within the neuronal upregulated genes. Downregulated genes were enriched for biological processes related to cell motility, inflammation, differentiation and proliferation (S13A–S13D Fig). Glial function is known to be affected by cellular activity and motility, with morphological changes reflecting changes in cellular function [64–66]. Together, these large changes in the transcriptomes of the three glial cell types is likely to impact their functions and could affect the formation of memory.

We next sought to understand how well GR-mediated gene induction could explain the glia-specific DSBs seen *in vivo*, and whether genes regulated through this pathway in neurons incur DSBs. Examining all γ H2AX-containing genes that were also upregulated in one of the cell types after corticosterone, we found that the vast majority (32/43; 74%) are regulated only in glia (Fig 5D). Thus, we have identified a glial-enriched pathway that may be incurring DSBs during CFC. Collectively, these results show that genes responsive to stress hormone are predominantly glial, with some of these genes showing high levels of the DSB marker γ H2AX and likely modulating important glial functions.

Discussion

There is increasing evidence for an association between neuronal activity and the generation of DSBs, but their *in vivo* location and relation to brain function is unknown [1–3, 5, 6]. Here, using γ H2AX as a proxy for DSBs, we identify hundreds of gene-associated DSBs in the medial

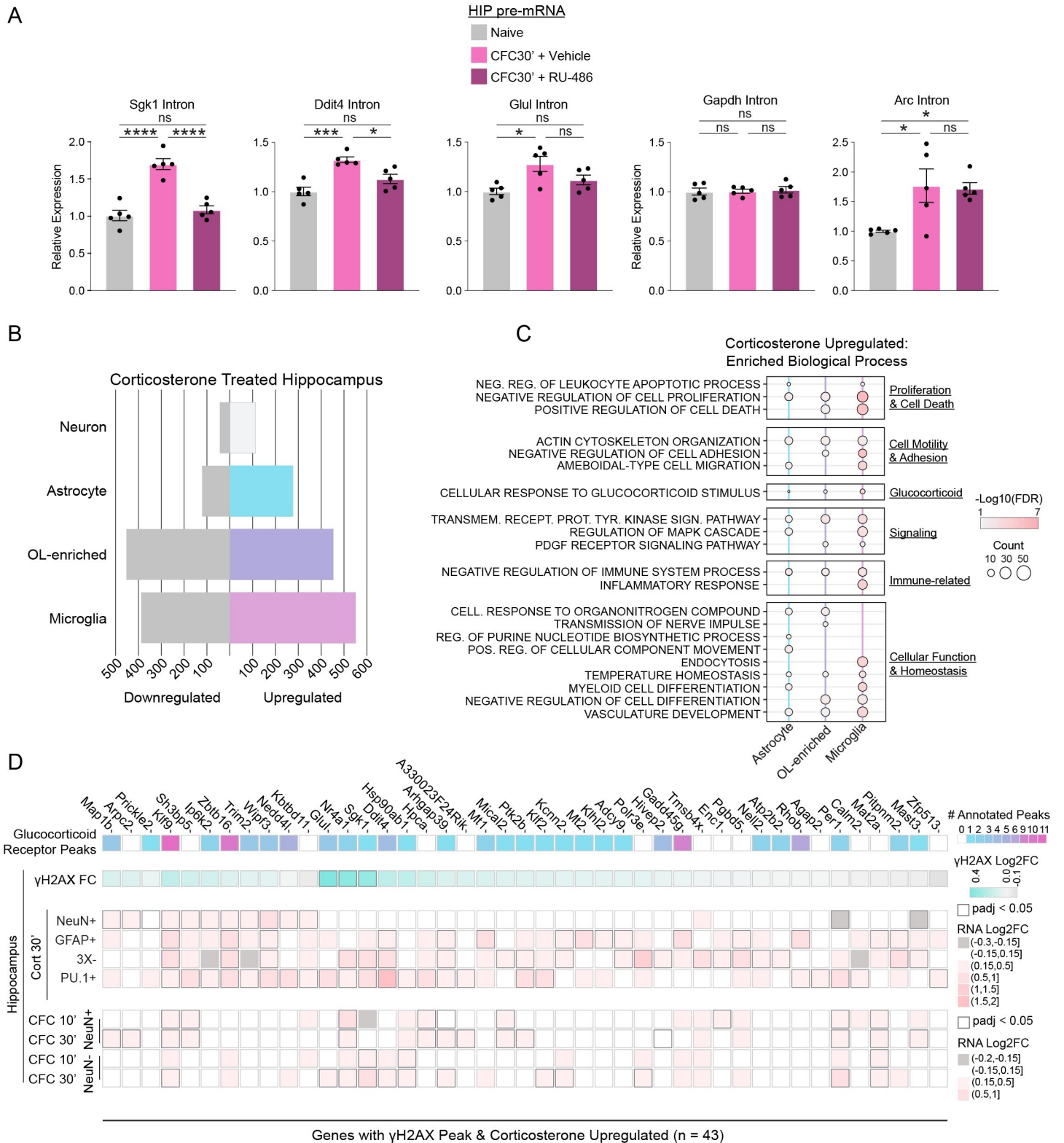


Fig 5. Glia, not neurons, have a robust transcriptional response to corticosterone. (A) Pretreatment with glucocorticoid receptor antagonist RU-486 (Mifepristone) blocks CFC-induced gene expression in hippocampus. Pretreatment with vehicle (1% v/v Tween 80 in saline) or 50 mg/kg RU-486 IP occurred 30 minutes prior to CFC. qRT-PCR analysis of pre-mRNA with intronic primer and normalized to *Hprt*. cDNA was primed with random hexamers. N = 5 mice per group; one-way ANOVA with Tukey's multiple comparisons test. (B) Number of corticosterone upregulated and downregulated genes from RNA-Seq of FACS-isolated nuclei from hippocampal cell

types 30 minutes after saline or corticosterone:HBC complex (2mg/Kg) treatment. Cutoff $\text{padj} < 0.05$. (C) Twenty-one representative top enriched biological processes for the upregulated genes in purified hippocampal nuclei from astrocytes, microglia, and oligodendrocyte-enriched after corticosterone treatment (276, 453, and 551 genes respectively; $\text{padj} < 0.05$). Summary categories representing each grouped list of GOs is listed on the right. No enrichment of processes at threshold $\text{padj} < 0.05$ with the 112 upregulated genes in neuronal nuclei. Over-representation analysis with gene ontology (GO) category "Biological Process." (D) Heatmap of 43 γH2AX peaks at genes upregulated in FACS-isolated neurons and glia following corticosterone treatment. From top: number of glucocorticoid receptor (GC) binding sites annotated per gene (rat cortical ChIP-Seq) [55, 56], γH2AX Log2FC in HIP after CFC, corticosterone-induced genes in NeuN+, GFAP+, PU.1+, and oligodendrocyte-enriched (3X-; NeuN-GFAP-PU.1-) hippocampal nuclear RNA-Seq 30 minutes after corticosterone treatment, and HIP RNA-Seq after CFC.

<https://doi.org/10.1371/journal.pone.0249691.g005>

prefrontal cortex and hippocampus that are important for learning and memory [16]. The surprisingly high number of genes with DSBs expands upon the small number previously observed in neurons following NMDA stimulation *in vitro* [3].

We observed that gene induction exhibits higher γH2AX than expected based on gene expression level, and disparate classes of γH2AX peaks, such as lincRNAs (*Lncpint*, *Mir9-3hg*, *Mir9-1hg*, *1700016P03Rik*[*mir212/mir132*]), housekeeping genes (*Hsp90ab1*, *Actb*), and as seen previously, lineage-specific genes [17], particularly those related to neuronal function (*Grin2b*, *Camk2a*, *Cck*, *Mbp*), are all regulated by CFC. However, though there is a clear correspondence between γH2AX peaks and CFC-induced genes, we do see less significant changes in γH2AX enrichment at many of these genes, with most of the peaks already present in the naive condition. In our previous study, significant γH2AX peaks become evident only after inducing neuronal activity in cultured neurons [3], suggesting that the presence of DSBs in the naive condition at known activity-induced genes may partially reflect basal neuronal activation occurring in the brain.

γH2AX is a sensitive marker of DSBs [67] that has been successfully used to map sites of DSBs occurring genome-wide through ChIP-Seq profiling [3, 17], including at known cleavage sites following the induction of restriction enzymes [18, 19, 68]. However, in some instances γH2AX is not reflective of underlying DSBs [69], including in neurons where pan-nuclear γH2AX staining was observed without evidence of DSBs during non-physiologic stimulation [70]. Additionally, two closely spaced single-strand DNA breaks (SSBs) could potentially be recognized as a DSB by the cell [71]. γH2AX increases following induction of SSBs in postmitotic neurons were dependent on transcription [72], suggesting that SSBs may require conversion to a DSB before generating a DNA damage response (DDR) and γH2AX formation [73]. While γH2AX ChIP-Seq has the benefit of measuring the DDR, profiling those DSBs in the genome that the cell recognizes as dangerous and in need of repair, it is important that methods which measure DNA breaks directly are utilized to both confirm the current results and to extend them through cell-type-specific analysis.

As most brain cells are postmitotic, they rely on non-homologous end joining (NHEJ) for DNA double-strand break (DSB) repair [25]. NHEJ can be error free, however, the presence of blocked DNA ends promotes end resection, which can result in sequence loss, rearrangements, or translocations [74]. The accumulation of irreversible sequence damage with time has the potential to perturb brain function during aging and disease [9], and efficient DNA repair pathways are thought to be critical to prevent functional decline during brain aging and neurodegeneration [25, 75]. ERGs and heat shock genes, two classes of DSB hotspots that were induced following CFC in neurons and non-neurons, were found in the aged pancreas to be sites of transcriptional noise and this correlated with the presence of somatic mutations [76]. It is interesting to speculate whether the same process also occurs in the brain with age and whether it may compromise the brain's ability to respond to cellular insults occurring during aging or in neurodegeneration, where protein folding factors are upregulated during disease progression [77]. Whether their overexpression contributes to the accumulation of DNA breaks observed during the progression of neurodegenerative disease is unclear [70, 78]. Overall, we have identified sites of DSBs at genes important for neuronal and glial functions,

suggesting that impaired DNA repair of these recurrent DNA breaks which are generated as part of brain activity could result in genomic instability that contribute to aging and disease in the brain [9, 25].

Convergent transcription that leads to polymerase collision is known to generate DSBs [17, 79]. We observed a few instances in which small γ H2AX peaks are found near sites of antisense transcription. For example, a small γ H2AX peak is present within intron 1 of *Polr3e*, a known site of transcriptional interference between RNA polymerase II (Pol II) and antisense transcription mediated by RNA polymerase III (Pol III) (S14 Fig) [80]. Other examples include a small peak at *29000060B14Rik* that is within and antisense to *Clasp1*, the promoter of *Pcif1*, or other peaks which overlap the 3' UTRs of closely spaced genes (e.g., *Prrc2a/Bag6*, *Dbn1/Prr7*).

We found that glia are likely to play an underappreciated role in the response to stress in the nervous system and this corresponds with DSBs, a relation between stress hormones and DNA damage that was also observed in mouse fibroblasts [81]. Our results are reminiscent of observations in the nucleus accumbens after morphine treatment, where oligodendrocytes in particular were found to induce a number of genes targeted by the GR [82]. Why neurons exhibit such limited responses to corticosterone remains uncertain. However, given our observation that GR-bound enhancers are more active in glia, and that GR nuclear intensity increased in neurons after corticosterone treatment, it is likely that chromatin accessibility plays a key role determining the GR response, as reported previously [60]. This indicates a predominately epigenetic mechanism underpinning the modest transcriptional response that neurons exhibit to corticosterone.

We find that stress likely impacts the physiology of glia through modulation of their transcriptomes, impacting numerous cellular processes. These changes may explain how stress has been shown to impact glial morphology and function, including after CFC [50, 83–91]. The role of glucocorticoids during the brain's response to stress could therefore be partially separated into a predominantly non-transcriptional role in neurons, wherein the GR has an important transcription-independent function at the synapse that aids memory formation [59, 92]. In contrast, the homeostatic response to stress may run primarily through glia, consistent with the general role of glia in brain homeostasis. Beyond homeostasis, astrocytic GR expression was found to be necessary for CFC-induced memory formation [91], and future work will be required to better understand how glia facilitate or hinder learning through their GR response.

Our observations suggest that the glial contribution to the deleterious effects of stress hormones may be stronger than previously appreciated. This may include cases of steroid dementia, wherein cognitive alterations occur in response to high levels of glucocorticoids (e.g., Cushing's syndrome), as well as disorders characterized by anxiety and depression [93, 94]. Interestingly, the microglial gene expression signature seen after corticosterone treatment was enriched for disease associations such as inflammation and depression (S15 Fig). This fits with the observation that stress can potentiate the microglial inflammatory responses [95–97], and their implication in the etiology of depression [98]. Because we found that glial GR-bound enhancers are more active in responding to stress than those in neurons, we posit that susceptibility to stress may include an underappreciated genetic component comprised of glia-specific variants. This also implicates glia, particularly microglia, in the genetics of the many psychiatric and neurodegenerative disorders for which stress is a risk factor [99–102], including Alzheimer's disease [103, 104] and schizophrenia [105].

Materials and methods

Ethics statement

All mouse work was approved by the Committee for Animal Care of the Division of Comparative Medicine at Massachusetts Institute of Technology (protocol number 0618-044-21).

Contextual fear conditioning paradigm, treatments, and tissue collection

Sixty-eight 4-month-old C57BL6/J male mice were purchased from Jackson Laboratory (stock number 000664). Mice were group housed with a 12-hour light and dark cycle with access to food and water ad libitum. To minimize variability, mice were single housed for one week before experimental manipulation.

For contextual fear conditioning, mice were habituated in the context for 3 minutes prior to administration of 30 second-spaced dual 0.8 mA foot shocks applied by the grid floor. The animals remained in the chamber for an additional minute and were placed back in their home-cage. Ten or thirty minutes after placement in the context, mice were euthanized by cervical dislocation. For Mifepristone (Sigma-Aldrich) pretreatment, mifepristone was dissolved in 1% v/v Tween 80 in saline. Mice were treated IP with either 50mg/Kg mifepristone or vehicle immediately before contextual fear conditioning, followed by euthanasia 30 minutes later. For corticosterone treatment, corticosterone:HBC complex (Sigma-Aldrich) was dissolved in saline and administered at 2mg/Kg IP, or an equal volume of saline for control, followed by euthanasia 30 minutes later.

Treatment and control groups were euthanized in a staggered manner to minimize circadian differences between groups. Naive mice remained in their home cages prior to euthanasia. For tissue collection, the animals were sacrificed by cervical dislocation and the brains were rapidly extracted and submerged in ice-cold PBS. To isolate the medial prefrontal cortex and hippocampus, the brain was placed ventral side up in an Alto coronal 0.5mm mouse matrix resting on ice. Three coronal cuts were administered with razor blades, one separating the PFC from the olfactory bulb, one placed approximately around the optic chiasm to separate the PFC from the hippocampus, and one placed within the cerebellum for stability. The pieces containing the mPFC and hippocampi were placed in an ice-cold PBS-filled dish for isolation with a dissection microscope. To isolate the mPFC, a horizontal cut was administered just above the anterior olfactory nucleus with a razor blade. Two longitudinal cuts were made medial to the anterior forceps of the corpus callosum. Whole hippocampi were unfurled and isolated from within the cortex. White matter and either meninges, or choroid plexus [106], were removed to prevent contamination. Tissue was flash frozen in liquid nitrogen and stored at -80°C until processing.

Mixed glial cultures and treatments

For mixed glial cultures, four Swiss-Webster timed-pregnant mice were ordered from Charles River (stock number 024). Cortical glia from pups younger than postnatal day 6 were cultured essentially as described [107]. Briefly, cortices were dissociated with papain (Worthington Biochemical) and plated onto non-coated 10 cm petri dishes. Mixed glia were cultured for a minimum of one week in DMEM containing 10% FBS, GlutaMAX, and Pen-Strep at 37°C and 5% CO_2 . For treatment with glucocorticoid receptor agonist, dexamethasone (Sigma-Aldrich) was dissolved in DMSO and applied to the media at 100nM. For ChIP experiments, the cultured cells were fixed by diluting 16% Methanol-free Paraformaldehyde (Electron Microscopy Sciences) to 1% in the culturing media and rocked for 10 minutes, before quenching with 0.25M Tris pH 8 (a more effective quencher than glycine [108]). Cells were then scraped, and nuclei were released by resuspending in NF1 buffer (0.5% Triton X-100, 0.1M Sucrose, 5mM MgCl_2 , 1mM EDTA) and dounce-homogenized with a loose pestle for 30 strokes. Nuclei were centrifuged for 15 minutes 2000 RCF 4°C and the supernatant aspirated, leaving nuclei for downstream applications.

Tissue homogenization

Tissue was dissociated with a motorized pestle (Argos Technologies) in 0.3–0.5mL ice cold PBS treated with protease and phosphatase inhibitors (cOmplete & PhosSTOP; Roche). For

RNA isolation, RNase inhibitors were added to all buffers (RiboLock (Thermo Scientific) or SUPERaseIn (Invitrogen); 1:100 for homogenization, 1:1000 for buffers with BSA, and 1:10,000 for other buffers). Dissociated brain tissue was fixed in 10 mL of 1% Methanol-free Paraformaldehyde (16%; Electron Microscopy Sciences) for 10 minutes before quenching with 0.25M Tris-HCl pH 8 (a more effective quencher than glycine [108]). Homogenate was centrifuged for 15 minutes 2000 RCF 4°C and the supernatant aspirated. Nuclei were released by resuspending in NF1 buffer (0.5% Triton X-100, 0.1M Sucrose, 5mM MgCl₂, 1mM EDTA) and dounce-homogenized with a loose pestle for 30 strokes, then filtered with 70uM cell strainers (Falcon). Nuclei were centrifuged for 15 minutes 2000 RCF 4°C and the supernatant aspirated, leaving nuclei for downstream applications.

Whole-cell mRNA processing

Extraction of mRNA from whole tissue and cultured mixed glia was performed with the RNeasy mini kit (Qiagen). For brain tissue, homogenization was performed by aspirating the tissue in RLT Plus buffer through a 20-gauge needle and syringe approximately 10 times until homogenized. For cell culture, the media was aspirated before RLT Plus was added and distributed with rocking. Purification proceeded as described by the manufacturer. Isolated RNA was quantified on a NanoDrop spectrophotometer (Thermo Fisher Scientific) and 1ug RNA was used to make cDNA with the OligodT RNA to cDNA EcoDry Premix (Takara) according to the manufacturer's instructions, before proceeding to qPCR analysis.

qPCR

For qPCR analysis, diluted cDNA or genomic DNA was subjected to quantitative real-time PCR in triplicate with the indicated primers using Ssofast EvaGreen Supermix (Bio-Rad) in a CFX Connect Real-Time System (Bio-Rad). For gene expression analysis, normalization was against *Hprt* using the $\Delta\Delta CT$ method. For ChIP, normalization was against Input. Primer sequences can be found in [S1 Table](#).

Flow cytometry

Fixed brain nuclei (see 'Tissue Homogenization') were resuspended in 1mL 0.5% BSA in PBS (IgG-Free, Protease-Free; Jackson ImmunoResearch). Nuclei were stained in Eppendorf tubes with the relevant antibodies rocking for 30–60 minutes at 4°C. For neuron and glia isolation, nuclei were stained with NeuN AF488 (1:1000; clone MAB377X; Millipore). For neuron and glial subtype isolation, nuclei were stained with NeuN AF488 (1:1000; clone MAB377X; Millipore), GFAP AF647 (1:200; clone GA5; Cell Signaling Technology), and PU.1 PE (1:200; clone 9G7; Cell Signaling Technology). To stain for the glucocorticoid receptor, nuclei were incubated with Polyclonal Glucocorticoid Receptor (2 ug; clone PA1-511A, Thermo Fisher Scientific) followed by Donkey anti-Rabbit IgG AF647 (0.5ug; A-31573; Thermo Fisher Scientific). To stain for HSF1 receptor, nuclei were incubated with anti-HSF1 (1:250; 4356S; Cell Signaling Technologies) followed by Donkey anti-Rabbit IgG AF647 (0.5ug; A-31573; Thermo Fisher Scientific). Nuclei were pelleted between steps by centrifugation for 10–15 minutes at 2000RCF at 4°C. Finally, to help gate for singlet nuclei, 1:1000 DAPI (Sigma-Aldrich) was added to the buffer just prior to flow cytometry. Nuclei were then run on a LSRII cytometer (BD Biosciences) or isolated with a BD FACSAria (BD Biosciences) cell sorter into 1% BSA PBS with inhibitors. The data was analyzed with FlowJo software (FlowJo LLC).

Nuclear RNA isolation, cDNA generation, and sequencing

FACS-isolated nuclei (see ‘Flow Cytometry’) were pelleted by centrifugation for 15 minutes at 2000RCF at 4°C. To decrosslink the nuclei, the RecoverAll Total Nucleic Acid Isolation Kit for FFPE (Thermo Fisher Scientific) was utilized following the manufacturer’s instructions. Briefly, nuclei were resuspended in 200uL digestion buffer with 4 uL protease (an equal volume of protease K (NEB) was substituted if the manufacturer-provided protease was exhausted) for 15 minutes at 50C, then 15 minutes at 80C. To isolate the RNA and eliminate most DNA prior to DNAase treatment, 800uL TRIzol LS (Invitrogen) was added, mixed well, and incubated for 5 minutes at room temperature before proceeding with isolation or freezing at -80C. 215uL chloroform was added to the solution and vortexed vigorously for 30 seconds before adding to a 5Prime Phase Lock Gel Heavy tube (Quantabio) and centrifuged for 15 minutes at 12,000g at 4C before transfer to an eppendorf tube. An equal volume of 100% ethanol (800uL) was added immediately and mixed well before proceeding to RNA isolation with the Direct-zol RNA Microprep Kit (Zymo Research). DNase treatment and RNA isolation proceeded according to the manufacturer’s instructions, before elution in 6–20uL water.

The generation of cDNA from the isolated nuclear RNA was performed with SuperScript III or IV (Invitrogen) according to the manufacturer’s instructions, priming with either random hexamer or oligo(dT) primers. Diluted cDNA was then utilized for qPCR (see ‘qPCR’).

For library preparation, RNA concentration and quality was assessed with a Fragment Analyzer (Agilent), yielding an RNA fragment distribution concentrated between approximately 200bp to 6000bp. RNA-Seq libraries were generated with the SMARTer Stranded Total RNA-Seq Kit—Pico Input Mammalian (v1 or v2; Takara) according to the manufacturer’s instructions. Because the RNA was already partially degraded during the fixation and decrosslinking procedure, the RNA fragmentation time was 90 seconds. Paired end sequencing was performed with a NextSeq500 at the MIT BioMicro Center.

ChIP and ChIP-seq

Performed similar to [109]. Pelleted nuclei from cultured mixed glia (see ‘Mixed Glial Cultures and Treatments’) or dissociated brain tissue combined from three different animals’ hippocampi or mPFC (see ‘Tissue Homogenization’), were lysed by the addition of 400 µl LB3 (1mM EDTA pH 8, 0.5mM EGTA pH 8, 10 mM Tris pH 8, 0.5% Sarkosyl solution) and split into 2 tubes and sonicated on ‘HIGH’ for 30–40 cycles (30” on and 30” off) in a Bioruptor bath sonicator (Diagenode). The immunoprecipitation was prepared by diluting 15–30ug of the chromatin into 1% Triton X-100, 0.1% sodium deoxycholate, 1 mM EDTA plus protease and phosphatase tablets (cOmplete & PhosSTOP; Roche) and preclearing with Protein A Dynabeads (Life Technologies) blocked with BSA. Then 5 ug anti-γH2AX (ab2893; Abcam) or 10 uL anti-HSF1 (clone 4356S; Cell Signaling Technologies) were added and the chromatin rotated overnight. BSA blocked Protein A Dynabeads (Life Technologies) were added and rocked for 4 hours before 4 washes with RIPA buffer (50 mM HEPES, pH 7.6, 10 mM EDTA, 0.7% sodium Deoxycholate, 1% NP-40, 0.5 M LiCl) and one wash with T₅₀E₁₀ buffer (50 mM Tris-HCl pH 8.0, 10 mM EDTA) before resuspending beads in T₅₀E₁₀S₁ buffer (50 mM Tris-HCl pH 8.0, 10 mM EDTA, 1% SDS) and heating to 65C for 15 minutes to elute DNA. After transferring to a new tube, DNA was decrosslinked by leaving at 65C for 5 hours to overnight. DNA was treated with Proteinase K (NEB) and RNase (Roche) before purification with phenol:chloroform:isoamyl-alcohol 1 Phase (VWR), 5Prime Phase Lock Gel Heavy tube (Quantabio), and glycogen (sigma Aldrich) to facilitate DNA pelleting. Resuspended ChIP and Input DNA was then used for qPCR or ChIP-Seq. Library preparation utilized a HyperPrep Kit (Kapa Biosystems) and NEXTFLEX DNA Barcodes (Perkin Elmer), with size selection

performed with Agencourt AMPure XP (Beckman Coulter). Libraries were sequenced on the Illumina HiSeq2000 at the MIT BioMicro Center. γ H2AX ChIP-Seq was performed with three or four biological replicates.

RNA-Seq analysis

To eliminate nucleotides that are part of the template-switching oligo as per the manufacturer's instructions (SMARTer Stranded Total RNA-Seq Kit—Pico Input Mammalian; v1 [mPFC] or v2 [HIP]; Takara), the first three nucleotides of the first sequencing read (Read 1) for kit v1 or the first three nucleotides of the second sequencing read (Read 2) for kit v2 were trimmed with Trimmomatic [110]. Trimmed reads were then aligned to the mouse genome GRCm38 (mm10) with HISAT2 [111] using default parameters. Picard MarkDuplicates (<http://broadinstitute.github.io/picard/>) was used to remove duplicate reads and the remaining reads sorted and indexed with SAMtools [112]. Read counts aligning to the entire gene body of each gene (introns and exons) were generated using featureCounts [113]. Analysis of differential gene expression and FPKM values were then performed with DESeq2 [114] in R, with significance determined with $\text{padj} < 0.05$, and $\text{FPKM} > 0.2$ in at least one time point. To assess successful isolation of brain cell types, aggregate expression of known cell type-enriched genes was determined by taking the geometric mean of the naive FPKM values for each cell type's gene set [28], calculating the Z-score, and plotting with the R package pheatmap. To make combined signal tracks, SAMtools [112] was used to down sample replicates to an equal number of reads, before merging and generating normalized signal tracks with deepTools [115]. Genome browser signal tracks were generated with IGV [116]. Plotting was done with the ggplot2 package in R.

ChIP-Seq analysis

ChIP-Seq reads were aligned to the mouse genome GRCm38 (mm10) with Bowtie2 [117] with default parameters. Picard MarkDuplicates (<http://broadinstitute.github.io/picard/>) was used to remove duplicate reads. Poorly aligned reads were then filtered out ($\text{MAPQ} > 10$) and the remaining reads sorted and indexed with SAMtools [112]. SAMtools [112] was used to down sample ChIP replicates to an equivalent number of reads before merging. Peaks were called with MACS2 [118] using a broad-cutoff of 0.00001. To get peaks more representative of the underlying signal, peaks were recalled with MACS2 using—broad-cutoff 0.1, and bedtools intersect [119] was used to get the overlap with the more stringently called peaks. Bedtools intersect [119] was then used to annotate peaks overlapping genes with a minimum of 50% overlap with the GRCm38.93 (mm10) GTF annotation file, with manual inspection of genome browser tracks for correction. Read counts for either gene bodies or called peaks were generated using featureCounts [113]. Analysis of differential peaks and RPKM values was then performed with DESeq2 [114] in R. MACS2 [118] was used to make read normalized (-SPMR) LogLR signal tracks and these were converted to the bigwig file format with bedGraphToBigWig [120]. Aggregate signal plots were generated with deepTools [115]. Venn diagrams of shared peaks was generated with the 'eurlerr' R package. Genome browser signal tracks were generated with IGV [116]. Plotting was done with the ggplot2 package in R.

For analysis of H3K27Ac data [57], FASTQ files were downloaded from the gene expression omnibus, accession code GSE74971. Replicates were combined before alignment and filtering, which proceeded as above. Normalized read coverage signal tracks were generated with deepTools [115].

Permutation testing was performed similar to [121]. Neuronal upregulated genes were divided into bins by expression level. Using these bins, 1000 iterations of random sampling

without replacement was conducted on all expressed genes. A weighted mean of average FPKM for the CFC 30-minute time point, accounting for the approximate neuronal (NeuN+; 60%) and non-neuronal (NeuN-; 40%) composition of whole tissue, was used as the gene expression level for each gene to allow comparison with the whole tissue γ H2AX ChIP-Seq. A P-value was then calculated as the fraction of permutations that had higher mean γ H2AX or RNA intensity than that for the observed upregulated genes. Plotting was done with the ggplot2 package in R.

GO and motif analysis

To find promoter TF motif overrepresentation, the ‘enricher’ function of the clusterProfiler R package [21] was utilized with the MSigDB database [32] through the msigdb R package using the category "C3" and subcategory "TFT" with a pvalueCutoff = 0.01 and all expressed genes for the pertinent condition used as background. To determine overrepresentation of biological process GOs, the ‘enrichGO’ function of clusterProfiler [21] was utilized with the org.Mm.eg.db Bioconductor annotation R package, with a pvalueCutoff = 0.01 and expressed genes used as background. Redundant GO categories were then removed with the clusterProfiler [21] function ‘simplify’, an implementation of GOSemSim [122], with similarity set at 0.7. Disease overrepresentation analysis utilized the DOSE R package [123] with a Q-value cutoff of 0.2 and expressed genes used as background. Plotting was done with the ggplot2 package in R. Clustering of related top GO terms was performed with the ‘emaplot’ function of the clusterProfiler [21].

Glucocorticoid receptor external dataset analysis

Glucocorticoid receptor ChIP-Seq peaks from rat were downloaded from supplementary tables of [55, 56] and UCSC liftover [120] was used to convert the coordinates to the mouse MM10 genome. Peaks were merged with bedtools [119]. The presence of a mouse glucocorticoid receptor motif was determined by scanning the DNA sequence of each peak, obtained through the R package biomaRt [124], for the presence of the “GCR_MOUSE.H11MO.0.A” motif from the HOCOMOCO motif collection [125] with of the FIMO tool [126] of the MEME Suite [127]. GREAT [128] was used to annotate these peaks to the mouse genome, using “single nearest gene” as the annotation parameter. Plots of aggregate H3K27Ac [57] (see ‘ChIP-Seq analysis’) signal at glucocorticoid receptor peaks were generated with deepTools [115].

Statistical analysis

Two-tailed unpaired student’s t-test and One-way ANOVA with Tukey’s multiple comparisons test were performed with GraphPad PRISM (Version 8). $P \leq 0.05$ was considered statistically significant. Bar and scatter plots show the Mean \pm SEM. Outliers were detected with ROUT (Q = 2%). Other statistical tests were performed in R, including the hypergeometric distribution test using the ‘phyper’ function, linear regression with the ‘lm’ function, and Welch’s ANOVA with Games-Howell post-hoc test with the ‘oneway’ function.

Supporting information

S1 Table. Sequence of primers.

(XLSX)

S2 Table. Genome-wide called γ H2AX peaks.

(XLSX)

S3 Table. Nuclear RNA-Seq analysis.

(XLSX)

S4 Table. Glucocorticoid receptor binding sites.

(XLSX)

S1 Fig. γ H2AX ChIP-Seq. (A) qRT-PCR analysis of *Npas4* and *Arc* mRNA expression in the hippocampus (HIP) and medial prefrontal cortex (mPFC) 30 minutes following contextual fear conditioning (CFC30'), normalized to *Hprt* and respective naive condition. N = 4 mice per group; two-tailed unpaired student's t-test; * $P \leq 0.05$; ** $P \leq 0.01$; *** $P \leq 0.001$; **** $P < 0.0001$; Mean \pm SEM. (B) Volcano plots of Log2FC versus Log10(FDR) of γ H2AX peaks and their corresponding genes for HIP (left) and mPFC (right). Upregulated indicates $FDR < 0.05$ and $\log_2FC > 0$, Downregulated indicates $FDR < 0.05$ and $\log_2FC < 0$, ns indicates $FDR > 0.05$. (C) Correlation between gene length and γ H2AX peak length with linear regression. Left is HIP, right is mPFC. (D) Enrichment map of the 27 enriched biological processes for the 206 γ H2AX peak-containing genes shared between HIP and mPFC in Fig 1A. Overrepresentation analysis with gene ontology (GO) category "Biological Process." (E) Hippocampal γ H2AX ChIP-qPCR analysis at the gene bodies of early response genes *Npas4*, *Nr4a1*, and housekeeping gene *B2M*. Each replicate was generated from the pooling of 3 animals' hippocampi. N = 3; IgG N = 2; two-tailed unpaired student's t-test; ns $P > 0.05$; * $P \leq 0.05$; ** $P \leq 0.01$; Mean \pm SEM.

(TIF)

S2 Fig. Extraction of enriched NeuN+ and NeuN- nuclei from mouse brain. (A) Flow cytometry dot-plots representative of the gating strategy used for isolating neuronal and non-neuronal nuclei from mouse brain for RNA-Seq. Appropriately sized (FSC vs SSC), singlet nuclei (DAPI+), were gated for the presence or absence of the neuronal nuclei marker NeuN (NeuN+). (B) qRT-PCR analysis of pre-mRNA transcription from the neuronal early response gene *Npas4* and mRNA for the early response gene *Arc*. RNA purified from FACS-isolated nuclei or whole mPFC homogenate after CFC. cDNA was primed with random hexamers and the primer used for qPCR was either intronic (*Npas4*) or spanned an exon-exon junction (*Arc*). Normalized to *Hprt* and relative to naive NeuN+ for *Npas4* or normalized to respective naive condition for *Arc*. N = 3–4 mice per group; One-way ANOVA with Tukey's multiple comparisons test; absence of an asterisk indicates $P > 0.05$; * $P \leq 0.05$; ** $P \leq 0.01$; *** $P \leq 0.001$; **** $P < 0.0001$; Mean \pm SEM.

(TIF)

S3 Fig. Nuclear RNA-seq after contextual fear conditioning. (A) Correspondence between RNA-Seq datasets and brain cell types. Marker gene sets for brain cell types was obtained from a previously published dataset [28], and the average expression of these genes was calculated (RPKM geometric mean) for the naive conditions. Z-score determined by row. (B-E) Volcano plots of Log2FC versus log10(FDR) of RNA-Seq from HIP NeuN- (A), HIP NeuN+ (B), mPFC NeuN- (C), and mPFC NeuN+ (D). Up-regulated indicates $FDR < 0.05$ and $\log_2(FC) > 0$, Down-regulated indicates $FDR < 0.05$ and $\log_2(FC) < 0$, ns indicates $FDR > 0.05$. (F-G) Number of upregulated genes in neuronal (F) and non-neuronal (G) nuclei 10 to 30 minutes following CFC (RNA-Seq; $FDR < 0.05$). Genes shared between HIP and mPFC are in grey (CFC10') and light grey (CFC30').

(TIF)

S4 Fig. Brain γ H2AX corresponds with rapid gene induction and expression level. (A) Percent overlap between genes containing a γ H2AX peak and those genes upregulated

($p_{adj} < 0.05$) in non-neuronal nuclei after CFC. Hypergeometric distribution test; *** $P \leq 0.001$; **** $P < 0.0001$. (B) DSBs increase with RNA expression level; mPFC CFC30 γ H2AX ChIP-Seq intensity at gene bodies versus percentile of mPFC NeuN+ CFC30' RNA expression. Welch's ANOVA with Games-Howell post-hoc test. (C) Confirming equivalent RNA expression levels between the observed (upregulated) genes and expected (randomly sampled) genes for the permutation testing. Distribution of mean RNA FPKM for 1000 permutations of random sampling, binned by RNA expression level. Lines are the mean RNA FPKM. mPFC 10 minutes after CFC (left), or 30 minutes after CFC (right). (TIF)

S5 Fig. RNA-Seq promoter-enriched motifs in neurons. (A-B) Top 10 enriched promoter motifs for the genes upregulated in NeuN+ CFC10' HIP (A) and NeuN+ CFC10' mPFC (B). Using the "Transcription Factor Targets" (TFT) gene set from the molecular signatures database (MSigDB). (C) Top 8 enriched promoter motifs for the genes upregulated in neuronal nuclei from HIP 30 minutes after CFC ($\text{Log}_2\text{FC} > 0$ & $\text{FDR} < 0.05$). Using the "Transcription Factor Targets" (TFT) gene set from the molecular signatures database (MSigDB). (D) Motifs associated with upregulated genes in HIP NeuN+ nuclei. Left, number of the indicated motifs associated with each gene's promoter. Center, γ H2AX Log_2FC , right, RNA-Seq Log_2 fold change 10 or 30 minutes after CFC. Using the TFT gene sets from MSigDB for each transcription factor motif. (TIF)

S6 Fig. γ H2AX peaks are not enriched at late response genes. Differentially regulated genes from visual cortex single-cell RNA-Seq that also contain γ H2AX peaks in mPFC (right), and their regulation in mPFC nuclear RNA-Seq (left). 'Neuron' encompasses excitatory and inhibitory neuron subtypes, 'Glia' includes all subtypes from oligodendrocytes, microglia, astrocytes, and oligodendrocyte precursor cells, while 'Vasculature' denotes endothelial, pericyte, and smooth muscle cell subtypes [42]. (TIF)

S7 Fig. CFC induces early response genes in non-neuronal nuclei. (A) Motifs associated with upregulated genes in non-neuronal nuclei from HIP (top) or mPFC (bottom). Left, number of the indicated motifs associated with each gene's promoter. Center, γ H2AX Log_2FC , right, RNA-Seq Log_2 fold change 10 or 30 minutes after CFC. Using the TFT gene sets from MSigDB for each transcription factor motif. (B-C) Enrichment map of the top enriched biological processes for the genes upregulated in HIP NeuN- (B) or mPFC NeuN- (C) nuclei 30 minutes after CFC. Over-representation analysis with gene ontology (GO) category "Biological Process." (TIF)

S8 Fig. Increased HSF1 activity following CFC. (A) HSF1 binding increases at the promoter regions of chaperones *Hsp90ab1* and *Hspa8*. *Actb*, which is not a HSF1 target but has similarly increased levels of γ H2AX and gene expression showed lower HSF1 binding. ChIP-qPCR of cortex 30 minutes following CFC. $N = 6-7$; One-way ANOVA with Tukey's multiple comparisons test; ns $P > 0.05$; * $P \leq 0.05$; ** $P \leq 0.01$; *** $P \leq 0.001$; Mean \pm SEM. (B) Increased HSF1 nuclear translocation in neurons and non-neurons after CFC in cortex. Top, representative fluorescence intensity histograms after CFC (naïve, grey; CFC30, red). Bottom, intensity of nuclear HSF1 after CFC was analyzed by flow cytometry; median fluorescence intensity (MFI) normalized to respective naïve condition. $N = 7$; two-tailed unpaired student's t-test; ** $P \leq 0.01$; *** $P \leq 0.001$; Mean \pm SEM. (TIF)

S9 Fig. Related to Fig 4. (A) qRT-PCR analysis of *Sgk1* and *Ddit4* mRNA expression in the HIP and mPFC 30 minutes following contextual fear conditioning—normalized to *Hprt* and respective naive condition. N = 4 mice per group; two-tailed unpaired student's t-test; ** $P \leq 0.01$; Mean \pm SEM. (B) ChIP-qPCR analysis of γ H2AX induction at select gene bodies in mouse glial primary cultures 30 minutes after treatment with dexamethasone (Dex) (100nM). N = 4 independent cultures; two-tailed unpaired student's t-test; ns $P > 0.05$; Mean \pm SEM. (C) Average H3K27ac signal of prefrontal anterior cingulate cortex (ACC) at glucocorticoid receptor binding sites (rat cortical ChIP-Seq) [55,56] containing the GC motif in mouse (n = 5591 peaks). H3K27ac ChIP-Seq of naive mouse ACC from NeuN+ or NeuN- isolated nuclei [57]. (D) Average H3K27ac signal at intergenic glucocorticoid receptor binding sites (rat cortical ChIP-Seq) [55,56] containing the GC motif in mouse (n = 1860 peaks). H3K27ac ChIP-Seq of mouse hippocampal CA1 region from NeuN+ or NeuN- isolated nuclei 1 hour after exposure to context, or CFC (shock) [57]. (E) Mean expression of the glucocorticoid receptor (*Nr3c1*) from naive nuclear RNA-Seq datasets. (F) Intensity of nuclear glucocorticoid receptor (left) or nuclear NeuN (right) in NeuN+ or NeuN- nuclei of the mPFC after corticosterone treatment. Normalized median fluorescence intensity (MFI). N = 5 mice per group; two-tailed unpaired student's t-test; ** $P \leq 0.01$; ns $P > 0.05$; Mean \pm SEM. (TIF)

S10 Fig. Purification and confirmation of glia cell types. (A) Flow cytometry dot-plots representative of the gating strategy used for isolating neuronal and glial nuclei from hippocampus for RNA-Seq. Appropriately sized (FSC vs SSC plot), singlet nuclei (DAPI+; DNA stain), are gated for the presence or absence of the neuronal nuclei marker NeuN (NeuN+); NeuN- nuclei are then separated by the astrocyte marker GFAP (GFAP+), GFAP- nuclei are then gated for the microglia marker P.1 (PU.1+), with the oligodendrocyte-enriched fraction, NeuN-/GFAP-/PU.1- (3X-), also collected. (B) RT-qPCR analysis of FACS-isolated nuclei for cell-type-specific markers: neuronal (*Npas4*), astrocyte (*Gfap*), microglial (*C1qa*), oligodendrocyte (*Mbp*). Normalized to *Hprt*; N = 8, 4 mice saline treated, 4 mice corticosterone treated. (C) Glucocorticoid receptor agonist corticosterone (Cort) induces *Sgk1*, *Ddit4*, and *Glul* in glia, and not the house-keeping gene *Actb*. RT-qPCR on FACS-purified hippocampal nuclear RNA from neurons (NeuN+), astrocytes (GFAP+), microglia (PU.1+), and oligodendrocytes-enriched (NeuN-GFAP-PU.1-; 3X-) 30 minutes after saline or corticosterone:HBC complex (2mg/Kg) administration. N = 4 mice per group; two-tailed unpaired student's t-test; * $P \leq 0.05$; *** $P \leq 0.001$; **** $P < 0.0001$; Mean \pm SEM.; * $P \leq 0.05$; *** $P \leq 0.001$; **** $P < 0.0001$. (TIF)

S11 Fig. Extensive corticosterone-mediated gene induction in the hippocampus. (A) Correspondence between hippocampal cell-type-specific RNA-seq datasets and brain cell types. Marker gene sets for brain cell types was obtained from a previously published dataset, and the average expression of these genes was calculated (RPKM geometric mean) for the saline condition [28]. Z-score determined by row. (B-E) Volcano plots of Log₂FC versus Log₁₀(FDR) of RNA-Seq from corticosterone treated hippocampal cell types. Upregulated indicates FDR < 0.05 and log₂(FC) > 0, Downregulated indicates FDR < 0.05 and log₂(FC) < 0, ns indicates FDR > 0.05. (TIF)

S12 Fig. Corticosterone induced biological process GO terms. (A-C) Enrichment map of the top 30 enriched biological processes for the genes upregulated in HIP after corticosterone treatment in astrocyte (A), oligodendrocyte-enriched (B), and microglia (C) nuclei. No enrichment in neurons. Over-representation analysis with gene ontology (GO) category "Biological

Process.”
(TIF)

S13 Fig. Corticosterone repressed biological process GO terms. (A-C) Enrichment map of the top enriched biological processes for the genes downregulated in HIP after corticosterone treatment in astrocytic (A), oligodendrocyte-enriched (B), and microglial (C) nuclei. Over-representation analysis with gene ontology (GO) category “Biological Process.” (D) Top five enriched biological processes of the downregulated genes for each cell type in purified hippocampal nuclei from neurons, astrocytes, microglia, and oligodendrocyte-enriched after corticosterone treatment ($\text{padj} < 0.05$). Over-representation analysis with gene ontology (GO) category “Biological Process.”
(TIF)

S14 Fig. γ H2AX peak at site of convergent transcription within gene *Polr3e*. Genome browser tracks for the gene *Polr3e* displaying a small (951bp) intronic γ H2AX peak in mPFC overlapping a mammalian interspersed repeat (MIR). MIR antisense transcription is shown on the negative strand (-).
(TIF)

S15 Fig. Enriched disease associations after corticosterone treatment. Enriched disease associations for the genes upregulated in HIP after corticosterone treatment in neuronal, astrocytic, microglial, and oligodendrocyte-enriched nuclei, filtered for disease associations related to the nervous system. An absent group indicates no enrichment at threshold $q < 0.05$. Over-representation analysis with DOSE Disease ontology.
(TIF)

Acknowledgments

We thank, Jay Penney, Hugh Cam, Matheus Victor, Omer Durak, Ping-Chieh Pao, Vishnu Dileep, and Ram Madabhushi for thoughtful comments and feedback on the manuscript; Jemie Cheng for nuclear FACS optimization; Ram Madabhushi and Jemie Cheng for ChIP guidance; Ping-Chieh Pao, Audrey Lee, and Chinnakkaruppan Adaikkan for experimental assistance; Ying Zhou for laboratory management; Erica McNamara for maintaining the mouse colony; the members of the Tsai laboratory for feedback and advice on this project.

Author Contributions

Conceptualization: Ryan T. Stott, Li-Huei Tsai.

Data curation: Ryan T. Stott.

Formal analysis: Ryan T. Stott.

Funding acquisition: Li-Huei Tsai.

Investigation: Ryan T. Stott, Oleg Kritsky.

Methodology: Ryan T. Stott.

Project administration: Li-Huei Tsai.

Supervision: Li-Huei Tsai.

Validation: Ryan T. Stott.

Visualization: Ryan T. Stott.

Writing – original draft: Ryan T. Stott.

Writing – review & editing: Ryan T. Stott, Oleg Kritsky, Li-Huei Tsai.

References

1. Suberbielle E, Sanchez PE, Kravitz A V., Wang X, Ho K, Eilertson K, et al. Physiologic brain activity causes DNA double-strand breaks in neurons, with exacerbation by amyloid- β . *Nat Neurosci*. 2013; 16: 613–21. <https://doi.org/10.1038/nn.3356> PMID: 23525040
2. Crowe SL, Movsesyan VA, Jorgensen TJ, Kondratyev A. Rapid phosphorylation of histone H2A.X following ionotropic glutamate receptor activation. *Eur J Neurosci*. 2006; 23: 2351–61. <https://doi.org/10.1111/j.1460-9568.2006.04768.x> PMID: 16706843
3. Madabhushi R, Gao F, Pfenning AR, Pan L, Yamakawa S, Seo J, et al. Activity-Induced DNA Breaks Govern the Expression of Neuronal Early-Response Genes. *Cell*. 2015; 161: 1592–1605. <https://doi.org/10.1016/j.cell.2015.05.032> PMID: 26052046
4. Zada D, Bronshtein I, Lerer-Goldshtein T, Garini Y, Appelbaum L. Sleep increases chromosome dynamics to enable reduction of accumulating DNA damage in single neurons. *Nat Commun*. 2019; 10: 1–12. <https://doi.org/10.1038/s41467-018-07882-8> PMID: 30602773
5. Crowe SL, Tsukerman S, Gale K, Jorgensen TJ, Kondratyev AD. Phosphorylation of histone H2A.X as an early marker of neuronal endangerment following seizures in the adult rat brain. *J Neurosci*. 2011; 31: 7648–7656. <https://doi.org/10.1523/JNEUROSCI.0092-11.2011> PMID: 21613478
6. Li X, Marshall PR, Leighton LJ, Zajackowski EL, Wang Z, Madugalle SU, et al. The DNA repair-associated protein gadd45 γ regulates the temporal coding of immediate early gene expression within the prefrontal cortex and is required for the consolidation of associative fear memory. *J Neurosci*. 2019; 39: 970–983. <https://doi.org/10.1523/JNEUROSCI.2024-18.2018> PMID: 30545945
7. Rogakou EP, Pilch DR, Orr AH, Ivanova VS, Bonner WM. DNA double-stranded breaks induce histone H2AX phosphorylation on serine 139. *J Biol Chem*. 1998; 273: 5858–5868. <https://doi.org/10.1074/jbc.273.10.5858> PMID: 9488753
8. Bellesi M, Bushey D, Chini M, Tononi G, Cirelli C. Contribution of sleep to the repair of neuronal DNA double-strand breaks: Evidence from flies and mice. *Sci Rep*. 2016; 6: 1–13. <https://doi.org/10.1038/s41598-016-0001-8> PMID: 28442746
9. Chow HM, Herrup K. Genomic integrity and the ageing brain. *Nature Reviews Neuroscience*. Nature Publishing Group; 2015. pp. 672–684. <https://doi.org/10.1038/nrn4020> PMID: 26462757
10. Navabpour S, Rogers J, McFadden T, Jarome TJ. Dna double-strand breaks are a critical regulator of fear memory reconsolidation. *Int J Mol Sci*. 2020; 21: 1–15. <https://doi.org/10.3390/ijms21238995> PMID: 33256213
11. Ju B-G, Lunnyak V V, Perissi V, Garcia-Bassets I, Rose DW, Glass CK, et al. A topoisomerase II β -mediated dsDNA break required for regulated transcription. *Science*. 2006; 312: 1798–802. <https://doi.org/10.1126/science.1127196> PMID: 16794079
12. Lin C, Yang L, Tanasa B, Hutt K, Ju B, Ohgi K, et al. Nuclear receptor-induced chromosomal proximity and DNA breaks underlie specific translocations in cancer. *Cell*. 2009; 139: 1069–83. <https://doi.org/10.1016/j.cell.2009.11.030> PMID: 19962179
13. Morrow BA, Elsworth JD, Inglis FM, Roth RH. An antisense oligonucleotide reverses the footshock-induced expression of fos in the rat medial prefrontal cortex and the subsequent expression of conditioned fear-induced immobility. *J Neurosci*. 1999; 19: 5666–73. <https://doi.org/10.1523/JNEUROSCI.19-13-05666.1999> PMID: 10377372
14. Haffner MC, Aryee MJ, Toubaji A, Esopi DM, Albadine R, Gurel B, et al. Androgen-induced TOP2B-mediated double-strand breaks and prostate cancer gene rearrangements. *Nat Genet*. 2010; 42: 668–75. <https://doi.org/10.1038/ng.613> PMID: 20601956
15. Bunch H, Lawney BP, Lin YF, Asaithamby A, Murshid A, Wang YE, et al. Transcriptional elongation requires DNA break-induced signalling. *Nat Commun*. 2015; 6. <https://doi.org/10.1038/ncomms10191> PMID: 26671524
16. Maren S, Phan KL, Liberzon I. The contextual brain: Implications for fear conditioning, extinction and psychopathology. *Nature Reviews Neuroscience*. Nature Publishing Group; 2013. pp. 417–428. <https://doi.org/10.1038/nrn3492> PMID: 23635870
17. Boulianne B, Robinson ME, May PC, Castellano L, Blighe K, Thomas J, et al. Lineage-Specific Genes Are Prominent DNA Damage Hotspots during Leukemic Transformation of B Cell Precursors. *Cell Rep*. 2017; 18: 1687–1698. <https://doi.org/10.1016/j.celrep.2017.01.057> PMID: 28199841

18. Clouaire T, Rocher V, Lashgari A, Arnould C, Aguirrebengoa M, Biernacka A, et al. Comprehensive Mapping of Histone Modifications at DNA Double-Strand Breaks Deciphers Repair Pathway Chromatin Signatures. *Mol Cell*. 2018; 72: 250–262.e6. <https://doi.org/10.1016/j.molcel.2018.08.020> PMID: 30270107
19. Aymard F, Aguirrebengoa M, Guillou E, Javierre BM, Bugler B, Arnould C, et al. Genome-wide mapping of long-range contacts unveils clustering of DNA double-strand breaks at damaged active genes. *Nat Struct Mol Biol*. 2017; 24: 353–361. <https://doi.org/10.1038/nsmb.3387> PMID: 28263325
20. Iannelli F, Galbiati A, Capozzo I, Nguyen Q, Magnuson B, Michelini F, et al. A damaged genome's transcriptional landscape through multilayered expression profiling around in situ-mapped DNA double-strand breaks. *Nat Commun*. 2017; 8. <https://doi.org/10.1038/ncomms15656> PMID: 28561034
21. Yu G, Wang LG, Han Y, He QY. ClusterProfiler: An R package for comparing biological themes among gene clusters. *Omi A J Integr Biol*. 2012; 16: 284–287. <https://doi.org/10.1089/omi.2011.0118> PMID: 22455463
22. Lisman J, Yasuda R, Raghavachari S. Mechanisms of CaMKII action in long-term potentiation. *Nature Reviews Neuroscience*. Nature Publishing Group; 2012. pp. 169–182. <https://doi.org/10.1038/nrn3192> PMID: 22334212
23. Yap EL, Greenberg ME. Activity-Regulated Transcription: Bridging the Gap between Neural Activity and Behavior. *Neuron*. Cell Press; 2018. pp. 330–348. <https://doi.org/10.1016/j.neuron.2018.10.013> PMID: 30359600
24. Seeburg DP, Sheng M. Activity-induced polo-like kinase 2 is required for homeostatic plasticity of hippocampal neurons during epileptiform activity. *J Neurosci*. 2008; 28: 6583–6591. <https://doi.org/10.1523/JNEUROSCI.1853-08.2008> PMID: 18579731
25. Madabhushi R, Pan L, Tsai LH. DNA damage and its links to neurodegeneration. *Neuron*. Cell Press; 2014. pp. 266–282. <https://doi.org/10.1016/j.neuron.2014.06.034> PMID: 25033177
26. Mullen RJ, Buck CR, Smith AM. NeuN, a neuronal specific nuclear protein in vertebrates. *Development*. 1992; 116: 201–211. PMID: 1483388
27. Lin Y, Bloodgood BL, Hauser JL, Lapan AD, Koon AC, Kim TK, et al. Activity-dependent regulation of inhibitory synapse development by Npas4. *Nature*. 2008; 455: 1198–1204. <https://doi.org/10.1038/nature07319> PMID: 18815592
28. Habib N, Avraham-Davidi I, Basu A, Burks T, Shekhar K, Hofree M, et al. Massively parallel single-nucleus RNA-seq with DroNc-seq. *Nat Methods*. 2017; 14: 955–958. <https://doi.org/10.1038/nmeth.4407> PMID: 28846088
29. Schwer B, Wei P-CC, Chang AN, Kao J, Du Z, Meyers RM, et al. Transcription-associated processes cause DNA double-strand breaks and translocations in neural stem/progenitor cells. 2016; 113: 2258–2263. Available: <https://www.pnas.org/content/113/8/2258>
30. Lensing S V., Marsico G, Hänsel-Hertsch R, Lam EY, Tannahill D, Balasubramanian S. DSB-Capture: In situ capture and sequencing of DNA breaks. *Nat Methods*. 2016; 13: 855–857. <https://doi.org/10.1038/nmeth.3960> PMID: 27525976
31. Yan WX, Mirzazadeh R, Garnerone S, Scott D, Schneider MW, Kallas T, et al. BLISS is a versatile and quantitative method for genome-wide profiling of DNA double-strand breaks. *Nat Commun*. 2017; 8: 1–9. <https://doi.org/10.1038/s41467-016-0009-6> PMID: 28232747
32. Liberzon A, Subramanian A, Pinchback R, Thorvaldsdóttir H, Tamayo P, Mesirov JP. Molecular signatures database (MSigDB) 3.0. *Bioinformatics*. 2011; 27: 1739–1740. <https://doi.org/10.1093/bioinformatics/btr260> PMID: 21546393
33. Hawk JD, Bookout AL, Poplawski SG, Bridi M, Rao AJ, Sulewski ME, et al. NR4A nuclear receptors support memory enhancement by histone deacetylase inhibitors. *J Clin Invest*. 2012; 122: 3593–3602. <https://doi.org/10.1172/JCI64145> PMID: 22996661
34. Benito E, Valor LM, Jimenez-Minchan M, Huber W, Barco A. cAMP response element-binding protein is a primary hub of activity-driven neuronal gene expression. *J Neurosci*. 2011; 31: 18237–18250. <https://doi.org/10.1523/JNEUROSCI.4554-11.2011> PMID: 22171029
35. Bozon B, Davis S, Laroche S. A requirement for the immediate early gene zif268 in reconsolidation of recognition memory after retrieval. *Neuron*. 2003; 40: 695–701. [https://doi.org/10.1016/s0896-6273\(03\)00674-3](https://doi.org/10.1016/s0896-6273(03)00674-3) PMID: 14622575
36. Ramamoorthi K, Fropf R, Belfort GM, Fitzmaurice HL, McKinney RM, Neve RL, et al. Npas4 regulates a transcriptional program in CA3 required for contextual memory formation. *Science*. 2011; 334: 1669–75. <https://doi.org/10.1126/science.1208049> PMID: 22194569
37. Ramanan N, Shen Y, Sarsfield S, Lemberger T, Schütz G, Linden DJ, et al. SRF mediates activity-induced gene expression and synaptic plasticity but not neuronal viability. *Nat Neurosci*. 2005; 8: 759–767. <https://doi.org/10.1038/nn1462> PMID: 15880109

38. Nudelman AS, DiRocco DP, Lambert TJ, Garelick MG, Le J, Nathanson NM, et al. Neuronal activity rapidly induces transcription of the CREB-regulated microRNA-132, in vivo. *Hippocampus*. 2009; 20: NA-NA. <https://doi.org/10.1002/hipo.20646> PMID: 19557767
39. Kawashima T, Okuno H, Nonaka M, Adachi-Morishima A, Kyo N, Okamura M, et al. Synaptic activity-responsive element in the Arc/Arg3.1 promoter essential for synapse-to-nucleus signaling in activated neurons. *Proc Natl Acad Sci U S A*. 2009; 106: 316–321. <https://doi.org/10.1073/pnas.0806518106> PMID: 19116276
40. Hansen KF, Sakamoto K, Aten S, Snider KH, Loeser J, Hesse AM, et al. Targeted deletion of miR-132/-212 impairs memory and alters the hippocampal transcriptome. *Learn Mem*. 2016; 23: 61–71. <https://doi.org/10.1101/lm.039578.115> PMID: 26773099
41. Herschman HR. Primary Response Genes Induced by Growth Factors and Tumor Promoters. *Annu Rev Biochem*. 1991; 60: 281–319. <https://doi.org/10.1146/annurev.bi.60.070191.001433> PMID: 1883198
42. Hrvatin S, Hochbaum DR, Nagy MA, Cicconet M, Robertson K, Cheadle L, et al. Single-cell analysis of experience-dependent transcriptomic states in the mouse visual cortex. *Nat Neurosci*. 2018; 21: 120–129. <https://doi.org/10.1038/s41593-017-0029-5> PMID: 29230054
43. Morimoto RI. Regulation of the heat shock transcriptional response: Cross talk between a family of heat shock factors, molecular chaperones, and negative regulators. *Genes and Development*. Cold Spring Harbor Laboratory Press; 1998. pp. 3788–3796. <https://doi.org/10.1101/gad.12.24.3788> PMID: 9869631
44. Adamsky A, Kol A, Kreisel T, Doron A, Ozeri-Engelhard N, Melcer T, et al. Astrocytic Activation Generates De Novo Neuronal Potentiation and Memory Enhancement. *Cell*. 2018; 174: 59–71.e14. <https://doi.org/10.1016/j.cell.2018.05.002> PMID: 29804835
45. Mahat DB, Salamanca HH, Duarte FM, Danko CG, Lis JT. Mammalian Heat Shock Response and Mechanisms Underlying Its Genome-wide Transcriptional Regulation. *Mol Cell*. 2016; 62: 63–78. <https://doi.org/10.1016/j.molcel.2016.02.025> PMID: 27052732
46. Walter P, Ron D. The unfolded protein response: From stress pathway to homeostatic regulation. *Science*. American Association for the Advancement of Science; 2011. pp. 1081–1086. <https://doi.org/10.1126/science.1209038> PMID: 22116877
47. Yoshida H, Haze K, Yanagi H, Yura T, Mori K. Identification of the cis-acting endoplasmic reticulum stress response element responsible for transcriptional induction of mammalian glucose-regulated proteins: Involvement of basic leucine zipper transcription factors. *J Biol Chem*. 1998; 273: 33741–33749. <https://doi.org/10.1074/jbc.273.50.33741> PMID: 9837962
48. Yoshida H, Matsui T, Yamamoto A, Okada T, Mori K. XBP1 mRNA is induced by ATF6 and spliced by IRE1 in response to ER stress to produce a highly active transcription factor. *Cell*. 2001; 107: 881–891. [https://doi.org/10.1016/s0092-8674\(01\)00611-0](https://doi.org/10.1016/s0092-8674(01)00611-0) PMID: 11779464
49. Belmont PJ, Tadimalla A, Chen WJ, Martindale JJ, Thuerauf DJ, Marcinko M, et al. Coordination of growth and endoplasmic reticulum stress signaling by regulator of calcineurin 1 (RCAN1), a novel ATF6-inducible gene. *J Biol Chem*. 2008; 283: 14012–14021. <https://doi.org/10.1074/jbc.M709776200> PMID: 18319259
50. Miyata S, Koyama Y, Takemoto K, Yoshikawa K, Ishikawa T, Taniguchi M, et al. Plasma Corticosterone Activates SGK1 and Induces Morphological Changes in Oligodendrocytes in Corpus Callosum. Yoshikawa T, editor. *PLoS One*. 2011; 6: e19859. <https://doi.org/10.1371/journal.pone.0019859> PMID: 21655274
51. Wang Z, Malone MH, Thomenius MJ, Zhong F, Xu F, Distelhorst CW. Dexamethasone-induced gene 2 (dig2) is a novel pro-survival stress gene induced rapidly by diverse apoptotic signals. *J Biol Chem*. 2003; 278: 27053–27058. <https://doi.org/10.1074/jbc.M303723200> PMID: 12736248
52. Revest JM, Le Roux A, Roullot-Lacarrière V, Kaouane N, Vallée M, Kasanetz F, et al. BDNF-TrkB signaling through Erk1/2MAPK phosphorylation mediates the enhancement of fear memory induced by glucocorticoids. *Mol Psychiatry*. 2014; 19: 1001–1009. <https://doi.org/10.1038/mp.2013.134> PMID: 24126929
53. Heinzmann JM, Thoeringer CK, Knapman A, Palme R, Holsboer F, Uhr M, et al. Intrahippocampal corticosterone response in mice selectively bred for extremes in stress reactivity: A microdialysis study. *J Neuroendocrinol*. 2010; 22: 1187–1197. <https://doi.org/10.1111/j.1365-2826.2010.02062.x> PMID: 20735798
54. Mahfouz A, Lelieveldt BPF, Grefhorst A, Van Weert LTCM, Mol IM, Sips HCM, et al. Genome-wide coexpression of steroid receptors in the mouse brain: Identifying signaling pathways and functionally coordinated regions. *Proc Natl Acad Sci U S A*. 2016; 113: 2738–2743. <https://doi.org/10.1073/pnas.1520376113> PMID: 26811448

55. Polman JAE, De Kloet ER, Datson NA. Two populations of glucocorticoid receptor-binding sites in the male rat hippocampal genome. *Endocrinology*. 2013; 154: 1832–1844. <https://doi.org/10.1210/en.2012-2187> PMID: 23525215
56. Pooley JR, Flynn BP, Grøntved L, Baek S, Guertin MJ, Kershaw YM, et al. Genome-wide identification of basic helix-loop-helix and NF-1 motifs underlying GR binding sites in male rat hippocampus. *Endocrinology*. 2017; 158: 1486–1501. <https://doi.org/10.1210/en.2016-1929> PMID: 28200020
57. Halder R, Hennion M, Vidal RO, Shomroni O, Rahman RU, Rajput A, et al. DNA methylation changes in plasticity genes accompany the formation and maintenance of memory. *Nat Neurosci*. 2015; 19: 102–110. <https://doi.org/10.1038/nn.4194> PMID: 26656643
58. Kelly EJ, Sandgren EP, Brinster RL, Palmiter RD. A pair of adjacent glucocorticoid response elements regulate expression of two mouse metallothionein genes. *Proc Natl Acad Sci U S A*. 1997; 94: 10045–10050. <https://doi.org/10.1073/pnas.94.19.10045> PMID: 9294160
59. Chen DY, Bambah-Mukku D, Pollonini G, Alberini CM. Glucocorticoid receptors recruit the CaMKII α -BDNF-CREB pathways to mediate memory consolidation. *Nat Neurosci*. 2012; 15: 1707–1714. <https://doi.org/10.1038/nn.3266> PMID: 23160045
60. John S, Sabo PJ, Thurman RE, Sung MH, Biddie SC, Johnson TA, et al. Chromatin accessibility pre-determines glucocorticoid receptor binding patterns. *Nature Genetics*. 2011. pp. 264–268. <https://doi.org/10.1038/ng.759> PMID: 21258342
61. McReynolds JR, Taylor A, Vranjkovic O, Ambrosius T, Derricks O, Nino B, et al. Corticosterone Potentiation of Cocaine-Induced Reinstatement of Conditioned Place Preference in Mice is Mediated by Blockade of the Organic Cation Transporter 3. *Neuropsychopharmacology*. 2017; 42: 757–765. <https://doi.org/10.1038/npp.2016.187> PMID: 27604564
62. Gagne D, Pons M, Philibert D. RU 38486: A potent antiglyucocorticoid in vitro and in vivo. *J Steroid Biochem*. 1985; 23: 247–251. [https://doi.org/10.1016/0022-4731\(85\)90401-7](https://doi.org/10.1016/0022-4731(85)90401-7) PMID: 2864478
63. Piechota M, Korostynski M, Golda S, Ficek J, Jantas D, Barbara Z, et al. Transcriptional signatures of steroid hormones in the striatal neurons and astrocytes. *BMC Neurosci*. 2017; 18: 37. <https://doi.org/10.1186/s12868-017-0352-5> PMID: 28381250
64. Greenhalgh AD, David S, Bennett FC. Immune cell regulation of glia during CNS injury and disease. *Nature Reviews Neuroscience*. *Nature Research*; 2020. pp. 139–152. <https://doi.org/10.1038/s41583-020-0263-9> PMID: 32042145
65. Stevens B. Glia: much more than the neuron's side-kick. *Current biology: CB*. 2003. pp. R469–72. [https://doi.org/10.1016/s0960-9822\(03\)00404-4](https://doi.org/10.1016/s0960-9822(03)00404-4) PMID: 12814563
66. Salter MW, Beggs S. Sublime microglia: Expanding roles for the guardians of the CNS. *Cell*. *Cell Press*; 2014. pp. 15–24. <https://doi.org/10.1016/j.cell.2014.06.008> PMID: 24995975
67. Mah LJ, El-Osta A, Karagiannis TC. γ H2AX: A sensitive molecular marker of DNA damage and repair. *Leukemia*. *Nature Publishing Group*; 2010. pp. 679–686. <https://doi.org/10.1038/leu.2010.6> PMID: 20130602
68. Iannelli F, Galbiati A, Capozzo I, Nguyen Q, Magnuson B, Michelini F, et al. A damaged genome's transcriptional landscape through multilayered expression profiling around in situ-mapped DNA double-strand breaks. *Nat Commun*. 2017; 8. <https://doi.org/10.1038/ncomms15656> PMID: 28561034
69. Turinetto V, Giachino C. Multiple facets of histone variant H2AX: a DNA double-strand-break marker with several biological functions. *Nucleic Acids Res*. 2015; 43: 2489–98. <https://doi.org/10.1093/nar/gkv061> PMID: 25712102
70. Shanbhag NM, Evans MD, Mao W, Nana AL, Seeley WW, Adame A, et al. Early neuronal accumulation of DNA double strand breaks in Alzheimer's disease. *Acta Neuropathol Commun*. 2019; 7: 1–18. <https://doi.org/10.1186/s40478-018-0656-4> PMID: 30606247
71. Cannan WJ, Pederson DS. Mechanisms and Consequences of Double-Strand DNA Break Formation in Chromatin. *Journal of Cellular Physiology*. *Wiley-Liss Inc.*; 2016. pp. 3–14. <https://doi.org/10.1002/jcp.25048> PMID: 26040249
72. Sordet O, Redon CE, Guirouilh-Barbat J, Smith S, Solier S, Douarre C, et al. Ataxia telangiectasia mutated activation by transcription- and topoisomerase I-induced DNA double-strand breaks. *EMBO Rep*. 2009; 10: 887–893. <https://doi.org/10.1038/embor.2009.97> PMID: 19557000
73. Cristini A, Ricci G, Britton S, Salimbeni S, Huang S yin N, Marinello J, et al. Dual Processing of R-Loops and Topoisomerase I Induces Transcription-Dependent DNA Double-Strand Breaks. *Cell Rep*. 2019; 28: 3167–3181.e6. <https://doi.org/10.1016/j.celrep.2019.08.041> PMID: 31533039
74. Bétermier M, Bertrand P, Lopez BS. Is Non-Homologous End-Joining Really an Inherently Error-Prone Process? Jinks-Robertson S, editor. *PLoS Genet*. 2014; 10: e1004086. <https://doi.org/10.1371/journal.pgen.1004086> PMID: 24453986

75. White RR, Vijg J. Do DNA Double-Strand Breaks Drive Aging? *Molecular Cell*. Cell Press; 2016. pp. 729–738. <https://doi.org/10.1016/j.molcel.2016.08.004> PMID: 27588601
76. Enge M, Arda HE, Mignardi M, Beausang J, Bottino R, Kim SK, et al. Single-Cell Analysis of Human Pancreas Reveals Transcriptional Signatures of Aging and Somatic Mutation Patterns. *Cell*. 2017; 171: 321–330.e14. <https://doi.org/10.1016/j.cell.2017.09.004> PMID: 28965763
77. Mathys H, Davila-Velderrain J, Peng Z, Gao F, Mohammadi S, Young JZ, et al. Single-cell transcriptomic analysis of Alzheimer's disease. *Nature*. 2019; 570: 332–337. <https://doi.org/10.1038/s41586-019-1195-2> PMID: 31042697
78. Merlo D, Mollinari C, Racaniello M, Garaci E, Cardinale A. DNA Double Strand Breaks: A Common Theme in Neurodegenerative Diseases. *Curr Alzheimer Res*. 2016; 13: 1208–1218. <https://doi.org/10.2174/1567205013666160401114915> PMID: 27033054
79. Meng FL, Du Z, Federation A, Hu J, Wang Q, Kieffer-Kwon KR, et al. Convergent transcription at intragenic super-enhancers targets AID-initiated genomic instability. *Cell*. 2014; 159: 1538–1548. <https://doi.org/10.1016/j.cell.2014.11.014> PMID: 25483776
80. Yeganeh M, Praz V, Cousin P, Hernandez N. Transcriptional interference by RNA polymerase III affects expression of the Polr3e gene. *Genes Dev*. 2017; 31: 413–421. <https://doi.org/10.1101/gad.293324.116> PMID: 28289142
81. Flint MS, Baum A, Chambers WH, Jenkins FJ. Induction of DNA damage, alteration of DNA repair and transcriptional activation by stress hormones. *Psychoneuroendocrinology*. 2007; 32: 470–479. <https://doi.org/10.1016/j.psyneuen.2007.02.013> PMID: 17459596
82. Avey D, Sankararaman S, Yim AKY, Barve R, Milbrandt J, Mitra RD. Single-Cell RNA-Seq Uncovers a Robust Transcriptional Response to Morphine by Glia. *Cell Rep*. 2018; 24: 3619–3629.e4. <https://doi.org/10.1016/j.celrep.2018.08.080> PMID: 30257220
83. Murphy-Royal C, Johnston AD, Boyce AKJJ, Diaz-Castro B, Institoris A, Peringod G, et al. Stress gates an astrocytic energy reservoir to impair synaptic plasticity. *Nat Commun*. 2020; 11: 2014. <https://doi.org/10.1038/s41467-020-15778-9> PMID: 32332733
84. Choi M, Ahn S, Yang EJ, Kim H, Chong YH, Kim HS. Hippocampus-based contextual memory alters the morphological characteristics of astrocytes in the dentate gyrus. *Mol Brain*. 2016; 9: 72. <https://doi.org/10.1186/s13041-016-0253-z> PMID: 27460927
85. Kreisel T, Frank MG, Licht T, Reshef R, Ben-Menachem-Zidon O, Baratta M V., et al. Dynamic microglial alterations underlie stress-induced depressive-like behavior and suppressed neurogenesis. *Mol Psychiatry*. 2014; 19: 699–709. <https://doi.org/10.1038/mp.2013.155> PMID: 24342992
86. Chaaya N, Jacques A, Belmer A, Beecher K, Ali SA, Chehrehasa F, et al. Contextual fear conditioning alter microglia number and morphology in the rat dorsal hippocampus. *Front Cell Neurosci*. 2019; 13: 214. <https://doi.org/10.3389/fncel.2019.00214> PMID: 31139053
87. Tynan RJ, Naicker S, Hinwood M, Nalivaiko E, Buller KM, Pow D V., et al. Chronic stress alters the density and morphology of microglia in a subset of stress-responsive brain regions. *Brain Behav Immun*. 2010; 24: 1058–1068. <https://doi.org/10.1016/j.bbi.2010.02.001> PMID: 20153418
88. Koyanagi S, Kusunose N, Taniguchi M, Akamine T, Kanado Y, Ozono Y, et al. Glucocorticoid regulation of ATP release from spinal astrocytes underlies diurnal exacerbation of neuropathic mechanical allodynia. *Nat Commun*. 2016; 7. <https://doi.org/10.1038/ncomms13102> PMID: 27739425
89. Hinwood M, Morandini J, Day TA, Walker FR. Evidence that microglia mediate the neurobiological effects of chronic psychological stress on the medial prefrontal cortex. *Cereb Cortex*. 2012; 22: 1442–54. <https://doi.org/10.1093/cercor/bhr229> PMID: 21878486
90. Czéh B, Simon M, Schmelting B, Hiemke C, Fuchs E. Astroglial plasticity in the hippocampus is affected by chronic psychosocial stress and concomitant fluoxetine treatment. *Neuropsychopharmacology*. 2006; 31: 1616–1626. <https://doi.org/10.1038/sj.npp.1300982> PMID: 16395301
91. Tertilt M, Skupio U, Barut J, Dubovyk V, Wawrzczak-Bargiela A, Soltys Z, et al. Glucocorticoid receptor signaling in astrocytes is required for aversive memory formation. *Transl Psychiatry*. 2018; 8: 255. <https://doi.org/10.1038/s41398-018-0300-x> PMID: 30487639
92. Liston C, Cichon JM, Jeanneteau F, Jia Z, Chao M V., Gan WB. Circadian glucocorticoid oscillations promote learning-dependent synapse formation and maintenance. *Nat Neurosci*. 2013; 16: 698–705. <https://doi.org/10.1038/nn.3387> PMID: 23624512
93. Sacks O, Shulman M. Steroid dementia: an overlooked diagnosis?[see comment][summary for patients in *Neurology*. 2005 Feb 22; 64(4):E18–9; <https://doi.org/10.1212/wnl.64.4.e18> PMID: 15728273]. *Neurology*. 2005;64: 707–709.
94. Warrington TP, Bostwick JM. Psychiatric adverse effects of corticosteroids. *Mayo Clinic Proceedings*. Elsevier Ltd; 2006. pp. 1361–1367. <https://doi.org/10.4065/81.10.1361> PMID: 17036562

95. Frank MG, Thompson BM, Watkins LR, Maier SF. Glucocorticoids mediate stress-induced priming of microglial pro-inflammatory responses. *Brain Behav Immun*. 2012; 26: 337–345. <https://doi.org/10.1016/j.bbi.2011.10.005> PMID: 22041296
96. Munhoz CD, Lepsch LB, Kawamoto EM, Malta MB, De Sá Lima L, Avellar MCW, et al. Chronic unpredictable stress exacerbates lipopolysaccharide-induced activation of nuclear factor- κ B in the frontal cortex and hippocampus via glucocorticoid secretion. *J Neurosci*. 2006; 26: 3813–3820. <https://doi.org/10.1523/JNEUROSCI.4398-05.2006> PMID: 16597735
97. Duque E de A, Munhoz CD. The Pro-inflammatory Effects of Glucocorticoids in the Brain. *Front Endocrinol (Lausanne)*. 2016; 7. <https://doi.org/10.3389/fendo.2016.00078> PMID: 27445981
98. Yirmiya R, Rimmerman N, Reshef R. Depression as a Microglial Disease. *Trends in Neurosciences*. Elsevier Ltd; 2015. pp. 637–658. <https://doi.org/10.1016/j.tins.2015.08.001> PMID: 26442697
99. Cohen S, Murphy MLM, Prather AA. Ten Surprising Facts About Stressful Life Events and Disease Risk. *Annu Rev Psychol*. 2019; 70: 577–597. <https://doi.org/10.1146/annurev-psych-010418-102857> PMID: 29949726
100. Ludwig L, Paskan JA, Nicholson T, Aybek S, David AS, Tuck S, et al. Stressful life events and mal-treatment in conversion (functional neurological) disorder: systematic review and meta-analysis of case-control studies. *The Lancet Psychiatry*. 2018; 5: 307–320. [https://doi.org/10.1016/S2215-0366\(18\)30051-8](https://doi.org/10.1016/S2215-0366(18)30051-8) PMID: 29526521
101. Hollander JA, Cory-Slechta DA, Jacka FN, Szabo ST, Guilarte TR, Bilbo SD, et al. Beyond the looking glass: recent advances in understanding the impact of environmental exposures on neuropsychiatric disease. *Neuropsychopharmacology*. Springer Nature; 2020. pp. 1–11. <https://doi.org/10.1038/s41386-020-0648-5> PMID: 32109936
102. Wilson RS, Arnold SE, Schneider JA, Kelly JF, Tang Y, Bennett DA. Chronic psychological distress and risk of Alzheimer's disease in old age. *Neuroepidemiology*. 2006; 27: 143–153. <https://doi.org/10.1159/000095761> PMID: 16974109
103. Ouanes S, Popp J. High Cortisol and the Risk of Dementia and Alzheimer's Disease: A Review of the Literature. *Front Aging Neurosci*. 2019; 11. <https://doi.org/10.3389/fnagi.2019.00043> PMID: 30881301
104. Bisht K, Sharma K, Tremblay MÈ. Chronic stress as a risk factor for Alzheimer's disease: Roles of microglia-mediated synaptic remodeling, inflammation, and oxidative stress. *Neurobiology of Stress*. Elsevier Inc; 2018. pp. 9–21. <https://doi.org/10.1016/j.ynstr.2018.05.003> PMID: 29992181
105. Van Os J, Kenis G, Rutten BPF. The environment and schizophrenia. *Nature*. 2010. pp. 203–212. <https://doi.org/10.1038/nature09563> PMID: 21068828
106. Stankiewicz AM, Gosick J, Majewska A, Swiergiel AH, Juszczak GR. The Effect of Acute and Chronic Social Stress on the Hippocampal Transcriptome in Mice. Colombo GI, editor. *PLoS One*. 2015; 10: e0142195. <https://doi.org/10.1371/journal.pone.0142195> PMID: 26556046
107. O'Meara RW, Ryan SD, Colognato H, Kothary R. Derivation of enriched oligodendrocyte cultures and oligodendrocyte/neuron myelinating co-cultures from post-natal murine tissues. *J Vis Exp*. 2011. <https://doi.org/10.3791/3324> PMID: 21876528
108. Sutherland BW, Toews J, Kast J. Utility of formaldehyde cross-linking and mass spectrometry in the study of protein-protein interactions. *Journal of Mass Spectrometry*. *J Mass Spectrom*; 2008. pp. 699–715. <https://doi.org/10.1002/jms.1415> PMID: 18438963
109. Cheng J, Blum R, Bowman C, Hu D, Shilatifard A, Shen S, et al. A role for H3K4 monomethylation in gene repression and partitioning of chromatin readers. *Mol Cell*. 2014; 53: 979–992. <https://doi.org/10.1016/j.molcel.2014.02.032> PMID: 24656132
110. Bolger AM, Lohse M, Usadel B. Trimmomatic: a flexible trimmer for Illumina sequence data. *Bioinformatics*. 2014; 30: 2114–2120. <https://doi.org/10.1093/bioinformatics/btu170> PMID: 24695404
111. Kim D, Langmead B, Salzberg SL. HISAT: A fast spliced aligner with low memory requirements. *Nat Methods*. 2015; 12: 357–360. <https://doi.org/10.1038/nmeth.3317> PMID: 25751142
112. Li H, Handsaker B, Wysoker A, Fennell T, Ruan J, Homer N, et al. The Sequence Alignment/Map format and SAMtools. *Bioinformatics*. 2009; 25: 2078–2079. <https://doi.org/10.1093/bioinformatics/btp352> PMID: 19505943
113. Liao Y, Smyth GK, Shi W. featureCounts: an efficient general purpose program for assigning sequence reads to genomic features. *Bioinformatics*. 2013; 30: 923–930. <https://doi.org/10.1093/bioinformatics/btt656> PMID: 24227677
114. Love MI, Huber W, Anders S. Moderated estimation of fold change and dispersion for RNA-seq data with DESeq2. *Genome Biol*. 2014; 15: 550. <https://doi.org/10.1186/s13059-014-0550-8> PMID: 25516281

115. Ramírez F, Dündar F, Diehl S, Grüning BA, Manke T. deepTools: a flexible platform for exploring deep-sequencing data. *Nucleic Acids Res.* 2014; 42: W187–W191. <https://doi.org/10.1093/nar/gku365> PMID: 24799436
116. Robinson JT, Thorvaldsdóttir H, Winckler W, Guttman M, Lander ES, Getz G, et al. Integrative genomics viewer. *Nature Biotechnology.* Nature Publishing Group; 2011. pp. 24–26. <https://doi.org/10.1038/nbt.1754> PMID: 21221095
117. Langmead B, Salzberg SL. Fast gapped-read alignment with Bowtie 2. *Nat Methods.* 2012; 9: 357–359. <https://doi.org/10.1038/nmeth.1923> PMID: 22388286
118. Feng J, Liu T, Qin B, Zhang Y, Liu XS. Identifying ChIP-seq enrichment using MACS. *Nat Protoc.* 2012; 7: 1728–1740. <https://doi.org/10.1038/nprot.2012.101> PMID: 22936215
119. Quinlan AR, Hall IM. BEDTools: a flexible suite of utilities for comparing genomic features. *Bioinformatics.* 2010; 26: 841–842. <https://doi.org/10.1093/bioinformatics/btq033> PMID: 20110278
120. Kuhn RM, Haussler D, Kent WJ. The UCSC genome browser and associated tools. *Brief Bioinform.* 2012; 14: 144–161. <https://doi.org/10.1093/bib/bbs038> PMID: 22908213
121. Nicolae DL, Gamazon E, Zhang W, Duan S, Dolan ME, Cox NJ. Trait-Associated SNPs Are More Likely to Be eQTLs: Annotation to Enhance Discovery from GWAS. Gibson G, editor. *PLoS Genet.* 2010; 6: e1000888. <https://doi.org/10.1371/journal.pgen.1000888> PMID: 20369019
122. Yu G. Gene ontology semantic similarity analysis using GOSemSim. *Methods in Molecular Biology.* Humana Press Inc.; 2020. pp. 207–215. https://doi.org/10.1007/978-1-0716-0301-7_11 PMID: 31960380
123. Yu G, Wang L-G, Yan G-R, He Q-Y. DOSE: an R/Bioconductor package for disease ontology semantic and enrichment analysis. *Bioinformatics.* 2014; 31: 608–609. <https://doi.org/10.1093/bioinformatics/btu684> PMID: 25677125
124. Durinck S, Spellman PT, Birney E, Huber W. Mapping identifiers for the integration of genomic datasets with the R/Bioconductor package biomaRt. *Nat Protoc.* 2009; 4: 1184–1191. <https://doi.org/10.1038/nprot.2009.97> PMID: 19617889
125. Kulakovskiy I V, Vorontsov IE, Yevshin IS, Sharipov RN, Fedorova AD, Rumynskiy EI, et al. HOCO-MOCO: towards a complete collection of transcription factor binding models for human and mouse via large-scale ChIP-Seq analysis. *Nucleic Acids Res.* 2017; 46: D252–D259. <https://doi.org/10.1093/nar/gkx1106> PMID: 29140464
126. Grant CE, Bailey TL, Noble WS. FIMO: scanning for occurrences of a given motif. *Bioinformatics.* 2011; 27: 1017–1018. <https://doi.org/10.1093/bioinformatics/btr064> PMID: 21330290
127. Bailey TL, Boden M, Buske FA, Frith M, Grant CE, Clementi L, et al. MEME Suite: tools for motif discovery and searching. *Nucleic Acids Res.* 2009; 37: W202–W208. <https://doi.org/10.1093/nar/gkp335> PMID: 19458158
128. McLean CY, Bristol D, Hiller M, Clarke SL, Schaar BT, Lowe CB, et al. GREAT improves functional interpretation of cis-regulatory regions. *Nat Biotechnol.* 2010; 28: 495–501. <https://doi.org/10.1038/nbt.1630> PMID: 20436461